Environmental Science and Pollution Research (2022) 29:76003–76025
https://doi.org/10.1007/s11356-022-21217-7

RESEARCH ARTICLE

Pore-scale flow simulation of supercritical CO_2 and oil flow for simultaneous CO_2 geo-sequestration and enhanced oil recovery

Satyajit Chowdhury[1,2] · Mayank Rakesh[3] · Srawanti Medhi[2] · Japan Trivedi[4] · Jitendra S. Sangwai[1,5,6]

Received: 16 July 2021 / Accepted: 27 May 2022 / Published online: 4 June 2022

Abstract

Recently, carbon capture, utilization, and storage (CCUS) with enhanced oil recovery (EOR) have gained a significant traction in an attempt to reduce greenhouse gas emissions. Information on pore-scale CO_2 fluid behavior is vital for efficient geo-sequestration and EOR. This study scrutinizes the behavior of supercritical CO_2 (sc-CO_2) under different reservoir temperature and pressure conditions through computational fluid dynamics (CFD) analysis, applying it to light and heavy crude oil reservoirs. The effects of reservoir pressure (20 MPa and 40 MPa), reservoir temperature (323 K and 353 K), injection velocities (0.005 m/s, 0.001 m/s, and 0.0005 m/s), and in situ oil properties (835.3 kg/m^3 and 984 kg/m^3) have been considered as control variables. This study couples the Helmholtz free energy equation (equation of state) to consider the changes in physical properties of sc-CO_2 owing to variations in reservoir pressure and temperature conditions. It has been found that the sc-CO_2 sequestration is more efficient in the case of light oil than heavy oil reservoirs. Notably, an increase in temperature and pressure does not affect the trend of sc-CO_2 breakthrough or oil recovery in the case of a reservoir bearing light oil. For heavy oil reservoirs with high pressures, sc-CO_2 sequestration or oil recovery was higher due to the significant increase in density and viscosity of sc-CO_2. Quantitative analysis showed that the stabilizing factor (ε) appreciably varies for light oil at low velocities while higher sensitivity was displayed for heavy oil at high velocities.

Keywords Carbon capture and utilization · Computational fluid dynamics (CFD) · CO_2 geo-sequestration · Enhanced oil recovery (EOR) · Pore-scale investigation

Responsible Editor: Philippe Garrigues

✉ Jitendra S. Sangwai
jitendrasangwai@iitm.ac.in

[1] Gas Hydrate and Flow Assurance Laboratory, Petroleum Engineering Program, Department of Ocean Engineering, Indian Institute of Technology Madras, Chennai 600 036, India

[2] Assam Energy Institute, A Centre of Rajiv Gandhi Institute of Petroleum Technology, Sivasagar, Assam 785697, India

[3] Department of Petroleum Engineering and Earth Sciences, University of Petroleum and Energy Studies, Dehradun 248007, India

[4] Enhanced Oil Recovery and Reservoir Simulation Laboratory, School of Mining and Petroleum, Department of Civil and Environmental Engineering, University of Alberta, Edmonton, AB, Canada

[5] Department of Chemical Engineering, Indian Institute of Technology Madras, Chennai 600 036, India

[6] Center of Excellence on Subsurface Mechanics and Geo-Energy, Indian Institute of Technology Madras, Chennai 600 036, India

Introduction

Fossil fuels will remain to be a dominant source of energy for the coming decades (Xie and Economides 2009). The economical constraint over new hydrocarbon exploration activities has upsurged the development and deployment of enhanced oil recovery (EOR) methods. In depleted reservoirs, EOR techniques are implemented to maximize total oil recovery (Nwidee et al. 2016). Generally, a conventional hydrocarbon reservoir produces crude oil in three stages, namely primary, secondary, and tertiary stages. The tertiary stage refers to the production of crude oil by different EOR methods. Tertiary oil recovery or EOR can be implemented through several methods including thermal recovery (Gharibshahi et al. 2019), gas injection (Wang et al. 2018), chemical injection (Kumar et al. 2020; Sharma et al. 2016), low salinity waterflood (Behera and Sangwai 2020; Kakati et al. 2020; Seetharaman et al. 2020), microbial enhanced oil recovery (mEOR) (Sakthipriya et al. 2016; Yernazarova et al.

2016), and ultrasonic stimulation (Alvarado and Manrique 2010). These EOR methods are employed to increase the crude oil production so that the recovery factor could further increase (Tunio et al. 2011). However, the non-stop increasing demand and exploitation of fossil fuels as an energy source (85% of total energy needs) (El-hoshoudy and Desouky 2018) have posed an environmental threat due to increasing greenhouse gas (GHG) levels in the atmosphere. Carbon dioxide (CO_2) is one of the most significant components of GHG emissions (Sharma 2011). According to isotopic composition studies, at present, approximately 32 gigatons of CO_2 is released annually into the atmosphere (Huppert and Neufeld 2014). Generally, two possible solutions to mitigate this problem have been proposed, namely source-oriented methods and CO_2 storage and sink (Bachu 2000).

With new methods to utilize CO_2 and reduce its footprint, many methods to store these gases have emerged recently (Markewitz et al. 2012). Carbon capture and storage (CCS) also known as CO_2 sequestration inside geological formations is one of the prospective methods to mitigate CO_2 emissions in the atmosphere (Rutqvist 2012). CCS was first proposed by Marchetti (1977). Global warming and insufficient oil production from depleted reservoirs have led the scientific community to the development of CO_2 injection and sequestration as a method for EOR (Azzolina et al. 2016; Gaspar Ravagnani et al. 2009). Carbon dioxide can be entrapped inside the subsurface pore spaces by virtue of any of the following mediums: trapped beneath impermeable layers, trapped as an immobile phase, dissolved into formation fluids, adsorption onto the formation rocks, and organic matter such as shale (IPCC 2006; Ahmadi et al. 2016). The use of CO_2 for EOR is one of the most prominent methods of gas injection applications (Hashemi Fath and Pouranfard 2014). According to the study conducted by the Department of Energy (DOE), next-generation CO_2 EOR technologies can result in up to 137 billion barrels of additional technically recoverable oil from current reserves for the USA (Kuuskraa et al. 2011; Li et al. 2016). Previous studies revealed that CO_2 EOR processes can improve oil recovery by 7–23% of original oil in place (Martin and Taber 1992). Currently, the CO_2 EOR method contributes to 5% of the total USA's crude oil production (Enick et al. 2012). CO_2 EOR is also being implemented on a large field scale in China (Hill et al. 2020). Interestingly, CO_2 exists in a supercritical state below a depth of approximately 800 m and has a density of approximately 600 kg/m^3 (much higher as compared to 2 kg/m^3 at the surface) (van der Meer et al. 2009). CO_2 exists in a supercritical state under reservoir conditions of more than 7.38 MPa and 304.21 K (Carbon dioxide - gas encyclopedia air liquide | air liquide n.d.).

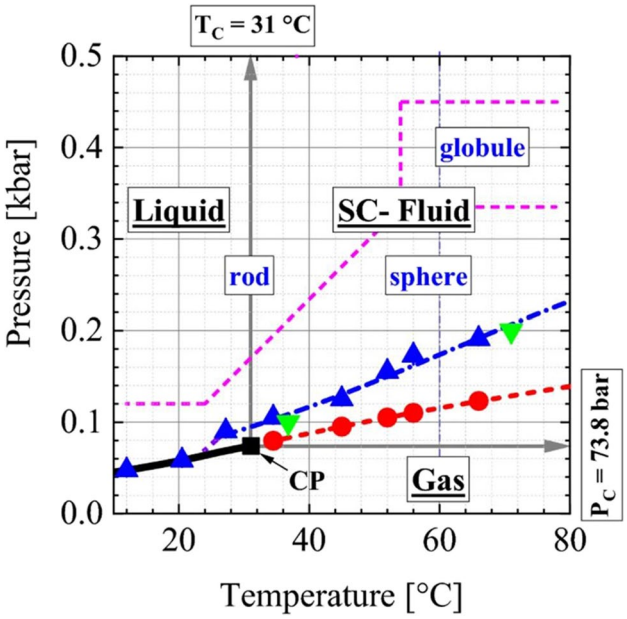

Fig. 1 Phases of CO_2 under different conditions of pressure and temperature (Pipich and Schwahn 2020)

Figure 1 represents the phase change in the state of CO_2 with varying pressure and temperature conditions (Witkowski et al. 2014). CO_2 at standard conditions (standard pressure and temperature, STP) generally behaves as gas, and at relatively higher pressures and low temperatures, it turns into solid ice. In case both pressure and temperatures get elevated, CO_2 follows a fine line between properties of gas and liquid (above the triple point). With a further increase in pressure and temperature, it reaches a critical point (7.377 MPa and 304.13 K) beyond which supercritical fluid nature dominates (Nikolai et al. 2019), where it expands like gas but

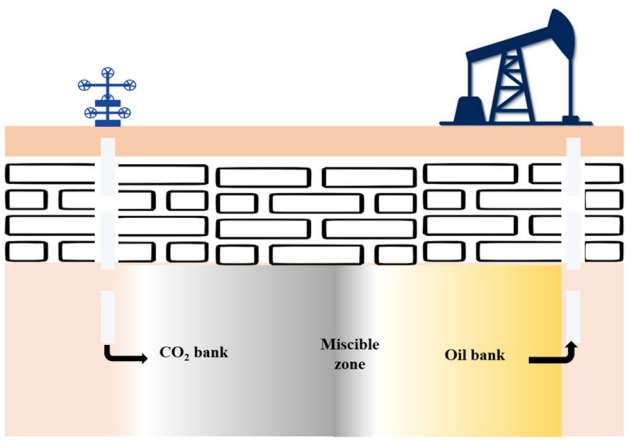

Fig. 2 Schematic representation of the sc-CO_2 miscible EOR process and mechanism

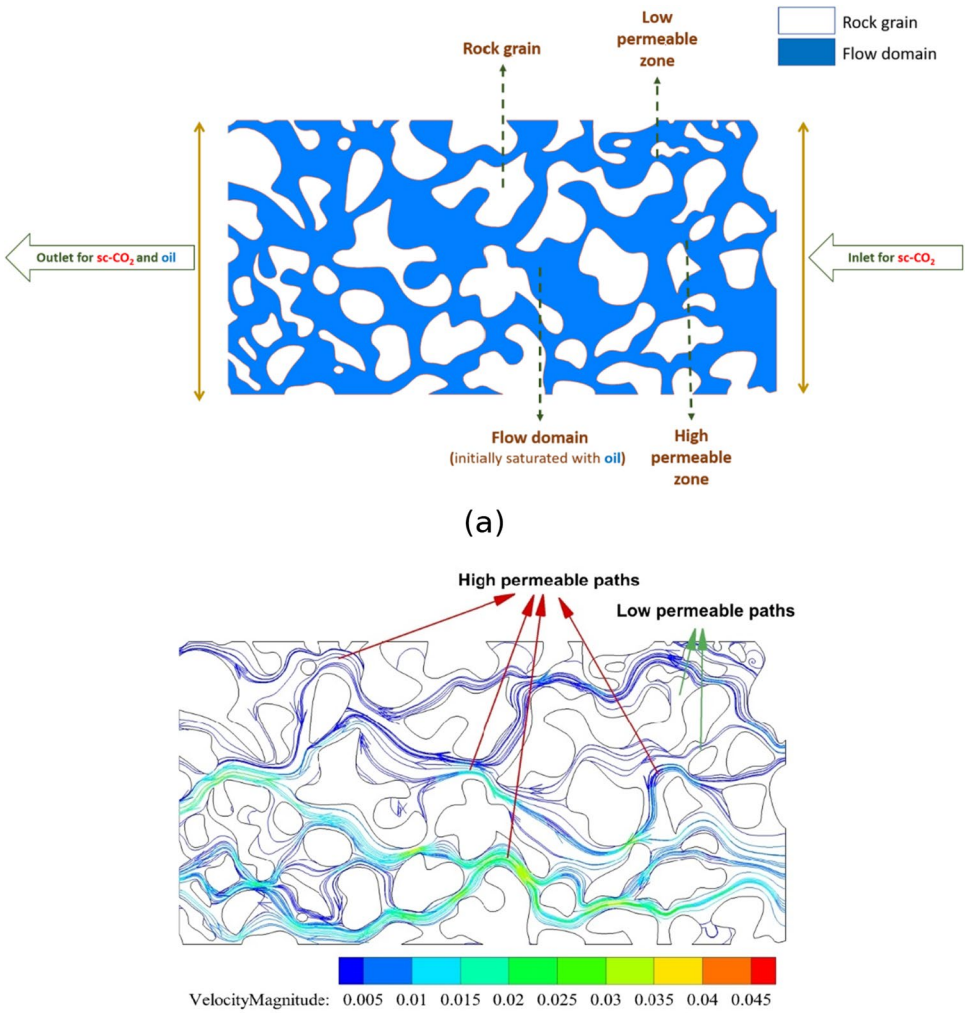

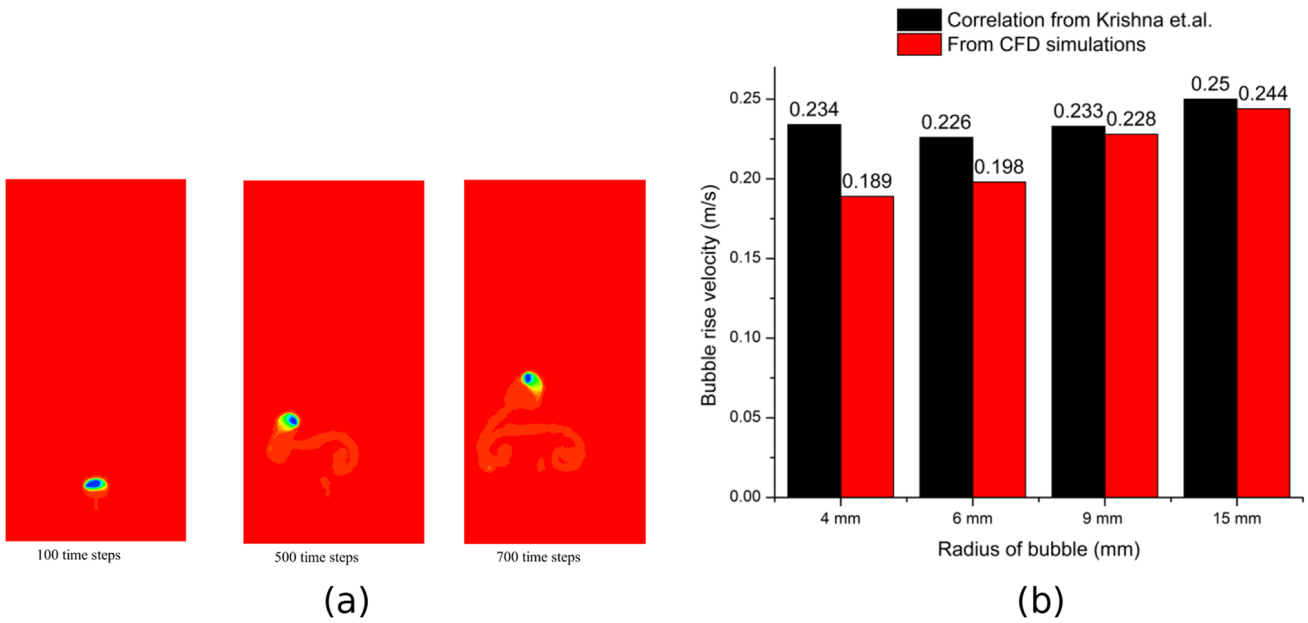

Fig. 3 **a** Porous model of 160 µm × 80 µm considered for the study. **b** Velocity streamtraces that distinguish high and low permeable paths

Fig. 4 Validation of the present numerical model with analytical correlation. **a** Time evolution of 4-mm air bubble inside the water tank. **b** Validation of CFD simulation for a rise of 4-mm, 6-mm, 9-mm, and 15-mm air bubbles

Validation by tracking and profile of the interface	Boundary conditions and other fluid properties
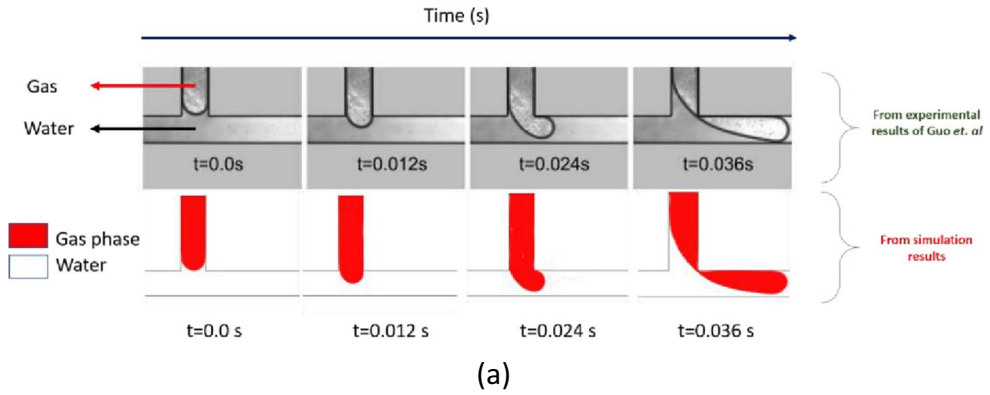	U_G = 0.035 m/s U_L 0.09 m/s Surface tension = 0.031 N/m Water wall contact angle = 0° where U_G and U_L are superficial velocities for gas and liquid respectively.
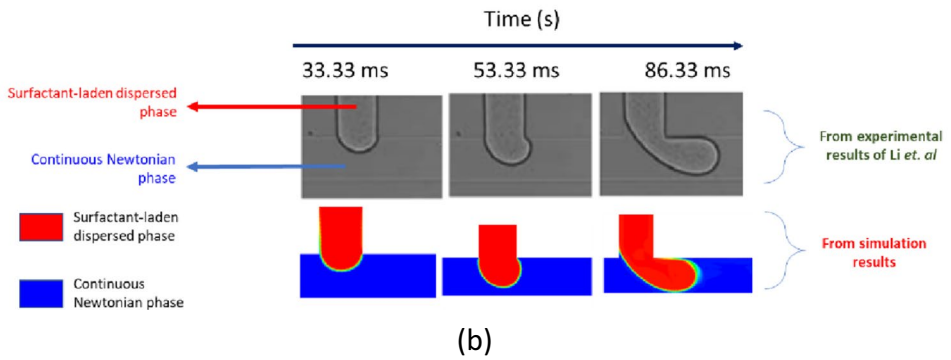	$V_c = V_d$ = 1.197 mm/s; μ_c = 44.1 mPa.s, μ_d = 1.05 mPa.s, Re = 0.00266, Ca = 0.0023. where μ_c and μ_d are viscosities of continuous and dispersed phase; Re is Reynolds number and C_a is capillary number

Fig. 5 Validation of numerical model used in this work for **a** the gas-liquid interaction from the experimental work reported by Guo and Chen (2009), where gas is the dispersed phase (being injected from top) and water in the continuous phase, and **b** the liquid-liquid interaction from the experimental work reported by Li et al. (2010), where surfactant (CTAC/NaSal aqueous solution) is the dispersed phase with silicon oil as the continuous phase

bears density like a liquid. The unique property that is achieved at the supercritical state is its solubility (Peach and Eastoe 2014). Although it behaves as a non-polar solvent, it has a restricted affinity for polar molecules due to its large quadrupole. One of the vital contrasts of supercritical fluids with conventional solvents is compressibility. The former required relatively smaller pressures and temperature changes to alter its density which provides convenience to the solvating process, as compared to conventional solvents.

Figure 2 describes a simplified process of supercritical CO_2 (sc-CO_2) EOR where sc-CO_2 is directed into the reservoir through an injection well (Sagir et al. 2018). The sc-CO_2 traverses through the pore spaces and interacts with the oil phase to form a miscible bank or zone that trails a concentrated oil bank, which is eventually displaced towards the producing well. The produced CO_2 gas phase is separated, recompressed, and re-injected to repeat the cycle of the displacement process. To understand and optimize the CO_2 EOR flooding technique, one must understand the fluid phase behavior of CO_2 under reservoir conditions and its interaction with formation fluids. After sc-CO_2 is injected into the reservoir, it becomes miscible (mutually soluble) with the in situ crude oil,

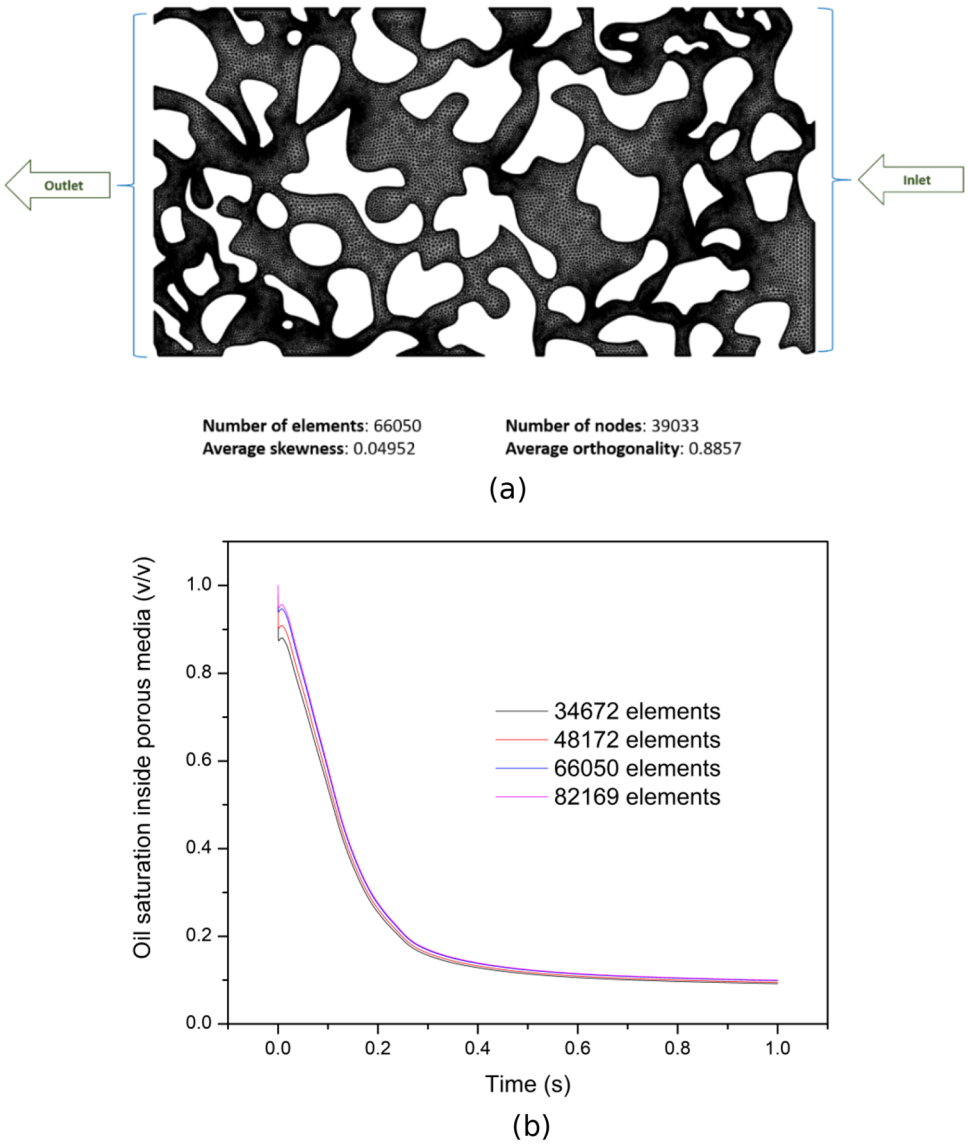

Fig. 6 **a** Free triangular mesh generated for simulation and mesh matrices. **b** Mesh sensitivity study at different mesh refinements

especially with the lighter fraction of the hydrocarbon. This phenomenon is predominant when the crude oil composition constitutes lighter components (low carbon) and when the density of sc-CO_2 is high. As the temperature of a reservoir increases, the density of sc-CO_2 decreases, and the density of oil increases due to the flashing of lighter hydrocarbons (Wang et al. 2018). This situation demands higher pressure to achieve oil/sc-CO_2 miscibility. This also hinders the mobility ratio and thereby reduces areal sweep efficiencies. Therefore, low-pressure reservoirs are poor candidates for sc-CO_2-driven EOR activities (Liu et al. 2019). However, repressurizing them with water before sc-CO_2 injection may be beneficial for efficient oil recovery. The physical force such as interfacial tension that exists between two immiscible phases (injection fluid and oil) disappears in the case of sc-CO_2 injection that allows it to penetrate the pore spaces of the reservoir rock and remove trapped residual oils (Wang et al. 2019). As sc-CO_2 dissolves into the oil phase, the overall displacement process is improved owing to swelling and reduction of viscosity of the oil. However, an interface pertains between sc-CO_2 and a heavier fraction of the crude oil, where miscibility of sc-CO_2 is difficult to achieve.

The interaction of sc-CO_2 and oil at the pore level is highly influenced by the local pressure and temperature continuum of the reservoir which subsequently dictates

Table 1 Cases considered for simulations (C1 to C18) in this study for sc-CO_2 geo-sequestration

Case no.[+]	Oil viscosity (kg/m/s)	Oil density (kg/m^3)	Reservoir pressure (MPa)	Reservoir temperature (K)	sc-CO_2 injection velocity (m/s)	Oil type
C1	0.0023811	835.3	20	323	0.005	Light oil
C2	0.0023811	835.3	20	323	0.001	
C3	0.0023811	835.3	20	323	0.0005	
C4	0.0023811	835.3	20	353	0.005	
C5	0.0023811	835.3	40	323	0.005	
C6	0.0023811	835.3	40	353	0.005	
C7	0.0023811	835.3	20	353	0.0005	
C8	0.0023811	835.3	40	323	0.0005	
C9	0.0023811	835.3	40	353	0.0005	
C10	0.048	984	20	323	0.005	Heavy oil
C11	0.048	984	20	323	0.001	
C12	0.048	984	20	323	0.0005	
C13	0.048	984	20	353	0.005	
C14	0.048	984	40	323	0.005	
C15	0.048	984	40	353	0.005	
C16	0.048	984	20	353	0.0005	
C17	0.048	984	40	323	0.0005	
C18	0.048	984	40	353	0.0005	

Case nos. 1 to 9 represent light oil study cases, and cases 10 to 18 represent heavy oil study cases

[+]In Table 1 and elsewhere in figures and text, C1 to C18 represent a case number defining the simulation runs and not composition

its physical property like density and viscosity. A study by Iglauer et al. (2019) shows that sc-CO_2 sequestration performs significantly better in oil-wet media. Injection velocity of the displacing fluid, as well as oil properties, also plays a crucial role in determining the extent of interaction of fluids inside the reservoir (Zhang et al. 2018). The trapping mechanism of CO_2 in porous media is in the form of cluster patches, and these structures are dependent upon reservoir conditions (Iglauer et al. 2011, 2016). Hence, a need to investigate the multiphase flow characteristics of oil and sc-CO_2 at a pore-scale level is deemed necessary. A capillary trapping phenomenon of supercritical fluids has been studied previously in the literature. In the study of Connolly et al. (2017), the trapping of nitrogen at reservoir conditions in various sandstone plugs was monitored using NMR. New advances in high-performance computing technologies have opened new doors to study and simulate different oil and gas upstream processes (Gharibshahi et al. 2015; Khalde et al. 2019; Medhi et al. 2020a, b; Ning et al. 2019; Zhao and Wen 2017) among which computational fluid dynamics (CFD) is a powerful method. Simulation of EOR techniques at the pore-scale network has enabled researchers to have an in-depth understanding of multiphase fluid flow behavior (Clemens et al. 2013; Guo et al. 2019; Zhao and Wen 2017). Several imaging techniques have also been adopted for geometry generation for pore-scale studies (Jha et al. 2020). CO_2 migration inside porous media for sequestration, fracturing, and EOR activities has been investigated in several studies (Li et al. 2017, 2019; Xu et al. 2020).

Past studies have proven CFD as an efficient modeling and simulation technique for CO_2 EOR methods. Simulation and optimization of CO_2 EOR in a reservoir for the Permian basin was conducted by Safi et al. (2016). The study concluded that the recovery factor can be significantly improved by optimizing the injection parameters such as well distance and injection velocity. However, this study was done at a macroscopic level. Choi et al. (2011) studied the numerical simulation of fluid flow and heat transfer of supercritical CO_2 flow inside a microporous media. The study investigated the effect of variable reservoir fluid properties on the performance of supercritical CO_2 injection, albeit for steady-state cases. Another study was conducted by Zhu et al. (2017) on CO_2 injection below critical conditions for a microporous oil-wet media. The study examined the flow conditions under different capillary numbers and gravity numbers. These limited studies imply that the change in sc-CO_2 physical properties inside porous media has not been considered during

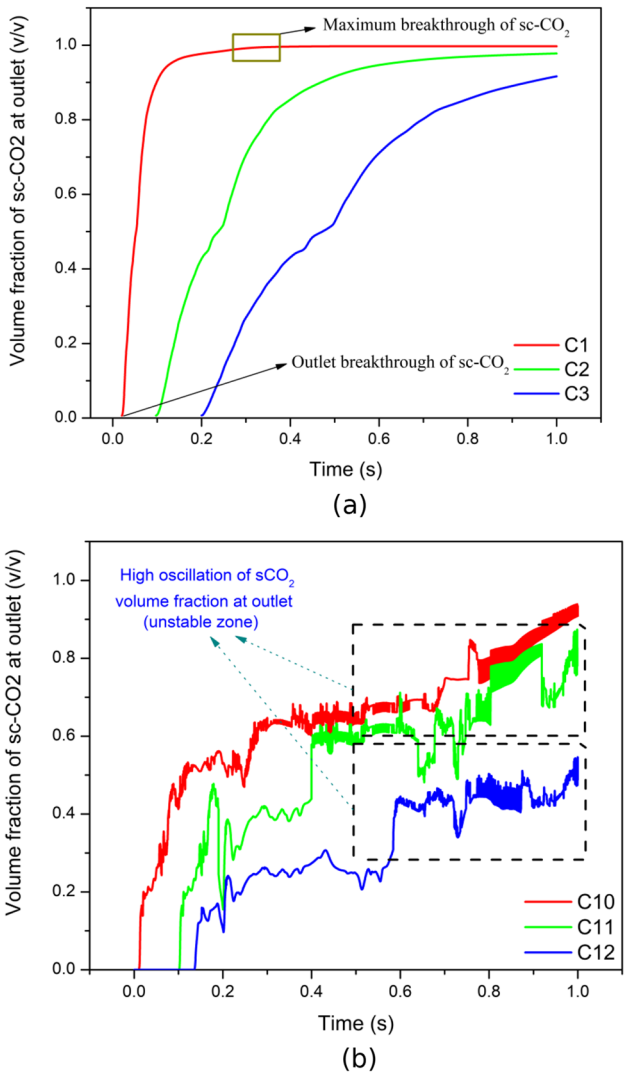

Fig. 7 sc-CO_2 breakthrough for **a** light crude oil for 0.005 m/s, 0.001 m/s, and 0.0005 m/s (C1–C3) inlet velocities and for **b** heavy crude oil for 0.005 m/s, 0.001 m/s, and 0.0005 m/s (C10–C12) inlet velocities

these studies. These alterations in physical properties like density and viscosity are vastly affected by the distinct pressure and temperature conditions found in different reservoirs. Moreover, random grain distribution inside the porous media was not considered for geometrical consideration. Although previous studies have reported the interaction of sc-CO_2 and water (Al-Zaidi et al. 2018; He et al. 2019), the interactivity of sc-CO_2 and oil also depends on injection velocities which were not considered along with changing physical properties of sc-CO_2.

This study aims to characterize the multiphase flow of sc-CO_2 and oil inside a 2-D randomly packed porous media (a replica of a typical oil reservoir) through an equation of state (EOS)–coupled CFD analysis. The control parameters considered in this study are reservoir temperature, reservoir pressure, sc-CO_2 injection velocity, and oil properties (light and heavy crude). The mathematical model for this study considers surface tension (low in magnitude) to define the oil-sc-CO_2 interface and incorporates a modified form of Helmholtz free energy equation (EOS) to capture the physical changes in sc-CO_2 due to changes in reservoir pressure and temperature. The governing equations of continuity, momentum, and energy are solved using the finite volume method in Ansys Fluent. Furthermore, results are presented in the form of surface integral of volume fraction at different locations and areas to analyze the extent of oil recovery or sc-CO_2 storage with a change in each control variable.

Geometry and computational details

Geometry model consideration

Figure 3a illustrates the model (porous domain) bearing 160 µm × 80 µm in dimension considered in this study. It consists of a random porous 2-D network having both low and high permeable zones as shown in Fig. 3b. The void spaces (pores) were initially patched with oil and are assigned as the flow domain. The entry of sc-CO_2 commences from the right side of the geometry and exits through the outlet present at the left. As sc-CO_2 proceeds, it displaces the oil from the pore spaces and corresponding volumes of oil and sc-CO_2 phases are obtained at the outlet.

Computational model

The flow of sc-CO_2 and its interaction with oil inside porous media is a complex process that is difficult to describe through algebraic equations or correlations, especially at a microscopic level. However, the governing equations such as continuity, momentum, and energy balance equations still hold and can be solved simultaneously inside a flow domain, numerically. The technique used in this study is the finite volume method which is vastly used to solve these governing equations for fluid flow problems. Unlike finite difference, it can deal with nonlinear heterogeneous boundaries that are found commonly in porous media. Four control parameters were studied in this investigation, namely reservoir pressure, reservoir temperature, sc-CO_2 injection velocities, and oil properties. These parameters highly influence the displacement efficiency and oil recovery that form the basis for the screening and design of sc-CO_2 EOR processes. The study,

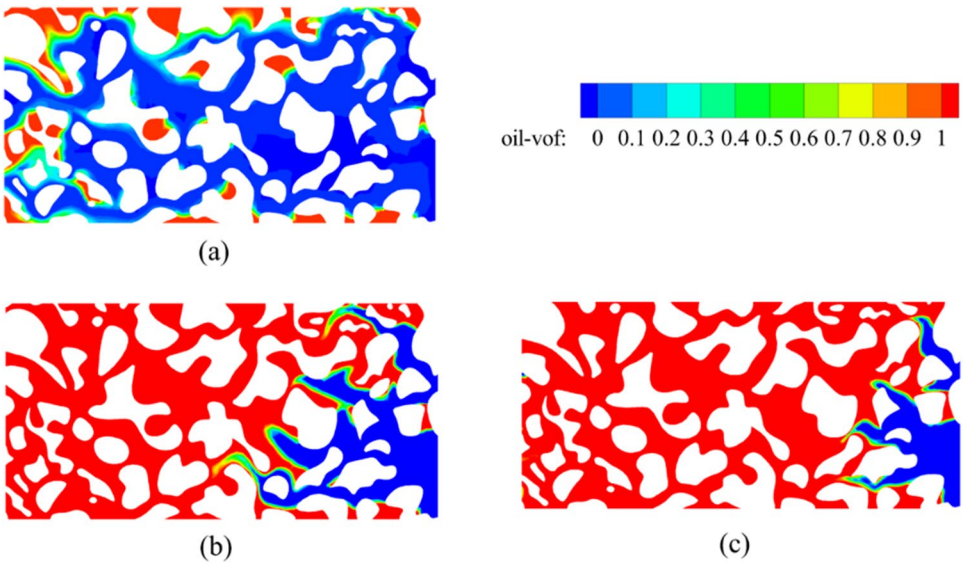

Fig. 8 sc-CO_2 injection at **a** C1 (0.005 m/s), **b** C2 (0.001 m/s), and **c** C3 (0.0005 m/s) for light crude oil at 0.05 s

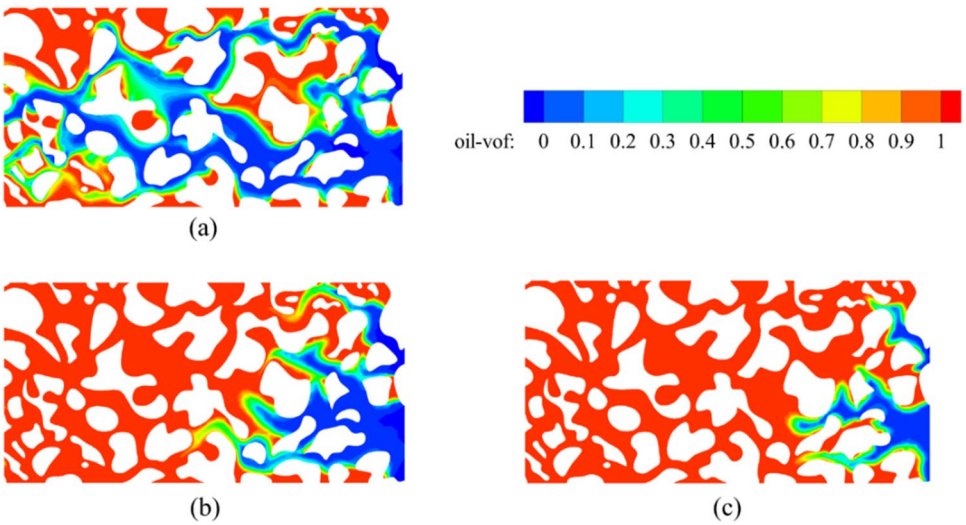

Fig. 9 sc-CO_2 injection at **a** C10 (0.005 m/s), **b** C11 (0.001 m/s), and **c** C12 (0.0005 m/s) for heavy crude oil at 0.05 s

however, does not capture the mass transfer between oil and sc-CO_2 and aims to seize only flow characteristics due to the change in abovementioned control parameters. A distinct boundary (to avoid complete mixing) was infused between the two phases by considering ultra-low interfacial tension (IFT). It has also been assumed that no heat transfer commences between the walls of the solid rock grain and the fluids involved as the reservoir is mostly considered in thermal equilibrium. sc-CO_2 is known to achieve partial miscibility with reservoir oil (Green and Paul Willhite 1998). An ultra-low interfacial tension is considered in this study as it shall have a distinct boundary with a heavier fraction of the oil present in the reservoir. This assumption also takes care of the fractional solubility of CO_2 in oil phase at supercritical conditions. The domain of study, numerical model, initial and boundary conditions, details of meshing, and other relevant pieces of information are described in the proceeding sections.

Mathematical model for flow simulation

Fluid flow behavior inside the porous flow domain was modeled using a multiphase model in Ansys Fluent. Conservation of momentum was characterized by Navier-Stokes (N-S) equation, and conservation of mass was defined using the continuity equation. The Navier-stokes equation (Prüss and Simonett 2010) is given as follows

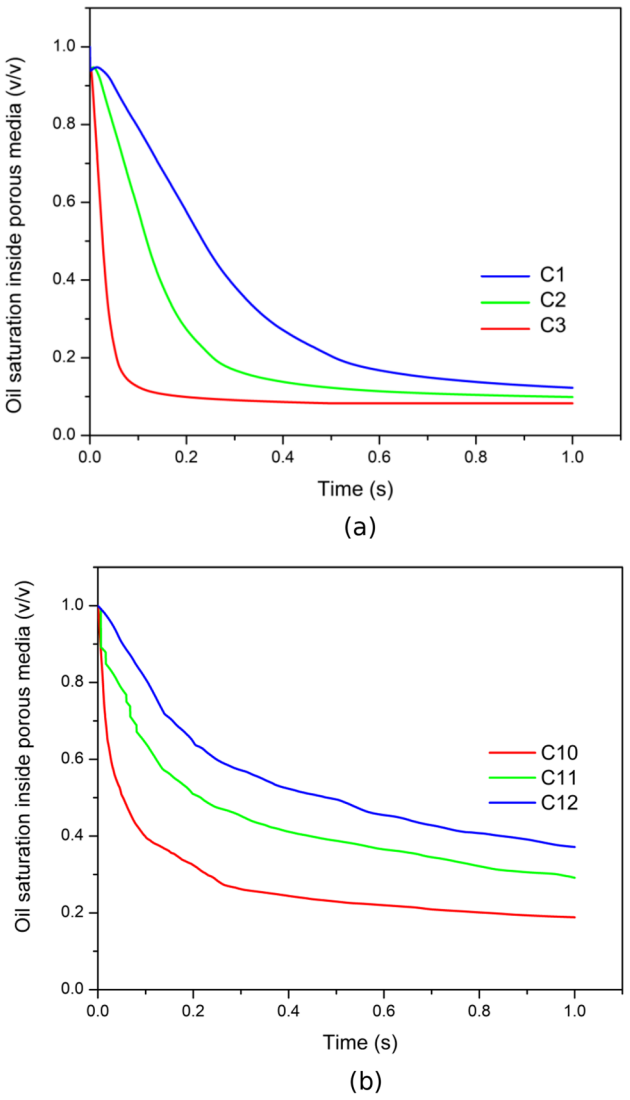

Fig. 10 Oil saturation decline (surface integral of volume fraction inside porous media) for **a** light oil for 0.005 m/s, 0.001 m/s, and 0.0005 m/s (C1–C3) inlet velocities and for **b** heavy oil for 0.005 m/s, 0.001 m/s, and 0.0005 m/s (C10–C12) inlet velocities

$$\frac{D\rho\vec{v}}{Dt} = -\nabla p + \nabla \cdots T + F_{\text{st}} \tag{1}$$

Left-hand side terms are convective momentum terms and represent the bulk transport of fluids. On the other hand, the right-side terms are diffusive momentum terms. Here, ρ is density (kg/m^3), and $\vec{v}$ is velocity vector (m/s). p and T refer to pressure energy and viscous stress tensor, respectively. F_{st} is the force due to the surface tension term and is defined by the continuum surface force (CSF) model (Brackbill et al. 1992). The CSF model resolves surface force numerically at fluid interfaces efficiently by the Eulerian approach. The interfacial surface force in a unit volume is expressed as (Lv and Wang 2015)

$$F_{\text{st}} = \sigma \frac{\rho k_1 \nabla \alpha_1}{\frac{1}{2}(\rho_1 + \rho_2)} \tag{2}$$

where σ is surface tension coefficient (N/m); ρ_1 and ρ_2 are the density of phase 1 and phase 2, respectively (kg/m^3); α_1 represents the volume fraction of phase 1; and k_1 is interface curvature. The continuity equation (Fanchi 2010) was defined as

$$\frac{D\rho}{Dt} + \rho(\nabla \cdots \vec{v}) = 0 \tag{3}$$

The fluid flow was modeled as compressible fluid; hence, density remained non-uniform throughout the flow domain. Interface tracking for the fluid-fluid interface was resolved using the volume of fluid (VOF) model (Hargreaves et al. 2007; Hirt and Nichols 1981). It is defined as

$$\left(\frac{\partial \alpha_1}{\partial t}\right) + \nabla \cdots (v\alpha_1) = 0 \tag{4}$$

where α_1 represents the volume fraction of phase 1 in a cell element.

Heat transfer between fluids and flow media was modeled by the energy equation (ANSYS n.d.). It is expressed as

$$\frac{\partial}{\partial t}(\rho E) + \nabla \cdot \left(\vec{v}(\rho E + p)\right) = \nabla \cdot K_{\text{eff}} \nabla T - \Sigma h_j \vec{J}_j + \left(\bar{\bar{\tau}} \cdot \vec{v}\right) + S_h \tag{5}$$

Here, terms on the right-hand side represent heat transfer by conduction, diffusion, and viscous dissipation, respectively. The viscosity change due to heat dissipation and pressure work was modeled by the above equation.

The properties of sc-CO_2 were modeled by the EOS as given by Span and Wagner (1996). It is based on the Helmholtz free energy equation and is considered to be efficient in resolving pressure-density-temperature relation. It is expressed as

$$\frac{A(\rho, T)}{RT} = \Phi(\delta, \tau) = \Phi^{\circ}(\delta, \tau) + \Phi^{\text{r}}(\delta, \tau) \tag{6}$$

where Φ is the dimensionless Helmholtz energy, ρ is density, T is temperature, R is gas constant, δ is reduced density (ratio of density and critical density), and τ is the reduced temperature (ratio of temperature and critical temperature). The equation has two components: residual behavior component (Φ^{r}) and ideal gas behavior component (Φ°). The residual component is defined as

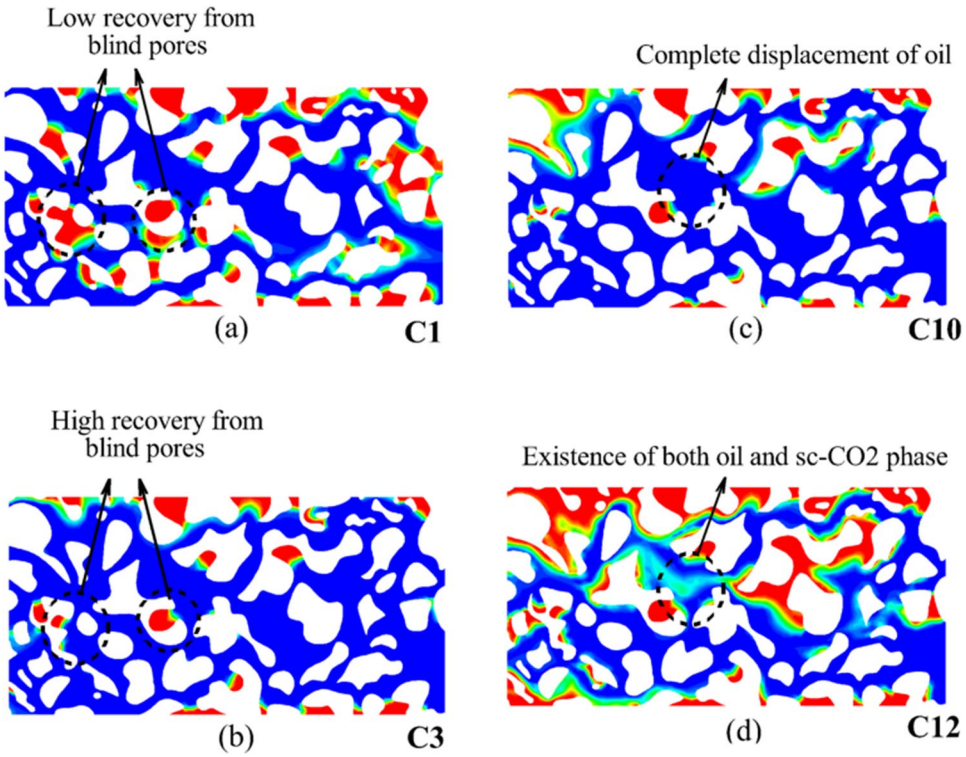

Fig. 11 Final sc-CO_2 sequestration in the porous network for light oil (**a** C1, **b** C3) and heavy oil (**c** C10, **d** C12)

$$\Phi^r = \sum_{i=1}^{7} n_i \delta^{d_i} \tau^{t_i} + \sum_{i=8}^{34} n_i \delta^{d_i} \tau^{t_i} e^{-\delta_i^c} + \sum_{i=35}^{39} n_i \delta^{d_i} \tau^{t_i} e^{-\alpha_i (\delta - \in_i)^2 - \beta_i (\tau - \gamma_i)^2} + \sum_{i=40}^{42} n_i \Delta^{b_i} \delta e^{-C_i (\delta - 1)^2 - D_i (\tau - 1)^2} \tag{7}$$

where n_i, d_i, t_i c, α_i, $\in_i$, β_i, γ_i, b_i, C_i, and D_i are coefficients and exponents. Refer to Table 31 of Span and Wagner (1996) for the corresponding values. The ideal gas component (Φ^r) is expressed as

$$\Phi^{\circ}(\delta, \tau) = \ln(\delta) + a_1^{\circ} + a_2^{\circ}\tau + a_3^{\circ} \ln(\tau) + \sum_{i=4}^{8} a_i^{\circ} \ln\left[1 - e^{(-\tau \Theta_i^{\circ})}\right] \tag{8}$$

where a_i° and Θ_i° are defined from elsewhere (Span and Wagner 1996).

The result variables were calculated in terms of area-weighted average over the area of interest. For any physical quantity "**Φ**" the area-weighted average is calculated by dividing the summation of the product of the selected field quantity and facet area with the total surface area. Mathematically, it is defined as

$$\frac{1}{A} \int \Phi dA = \frac{1}{A} \sum_{i=1}^{n} \Phi_i \mid A_i \mid \tag{9}$$

where A_i is the facet area and A is the total surface area.

Simulation strategy

The finite volume method (FVM) was used to solve the fluid flow and energy equations (Moukalled et al. 2016). The fluid flow domain was discretized to finite non-overlapping cell elements, and governing equations were integrated over these cell volumes. FVM is more accurate in fluid flow calculations as compared to the finite element method (FEM) due to its conservative nature and required less computational power (Jeong and Seong 2014; Molina-Aiz et al. 2010). Additionally, FVM works well for non-trivial and dynamic boundary conditions.

Numerical validation

The numerical model was validated against both analytical and experimental studies. Initially, the numerical model presented in the above section was validated by comparing results reported from the analytical work carried out by Krishna et al. (1999). The analytical model

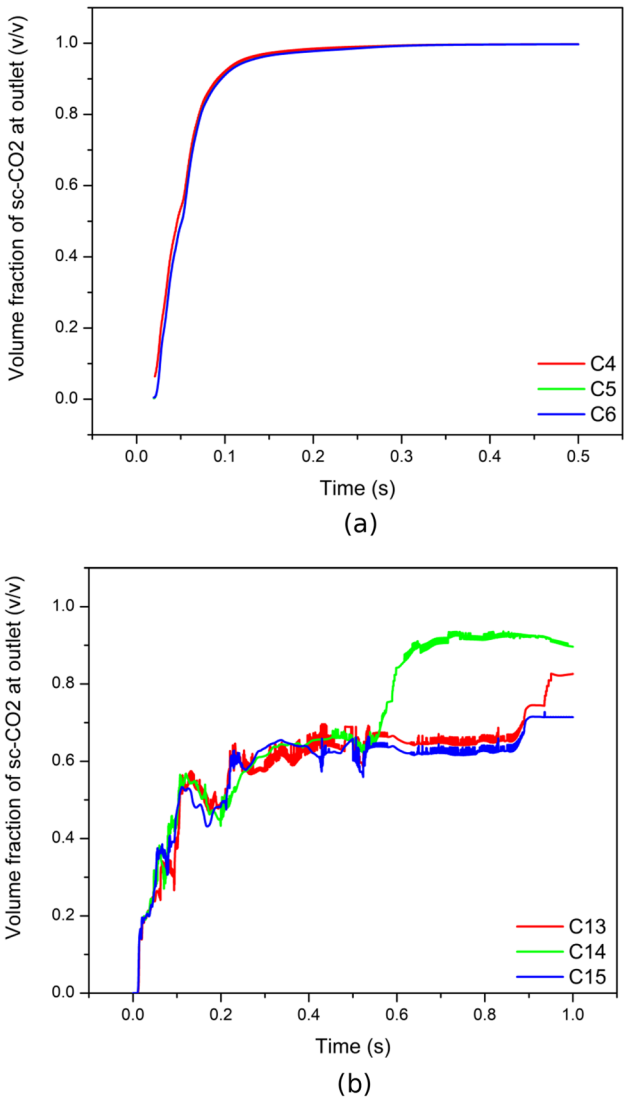

Fig. 12 Volume fraction of sc-CO_2 at the outlet for an sc-CO_2 inlet velocity of 0.005 m/s and different pressure and temperature conditions for **a** light oil (C4–C6) and **b** heavy oil (C13–C15)

used for validation is an extended form of the Mendelson equation (Mendelson 1967) which determines the terminal velocity of an air bubble rising in a tank filled with water. This approach was adopted for validation as the prime motive of this work is to track the fluid-fluid interface (between oil and sc-CO_2) during the displacement process. Figure 4 depicts the comparative analysis between the CFD results and analytical correlation using Eq. (10) (Krishna et al. 1999). A scale factor (SF) was introduced to take wall effects into account and is defined by

$$V_b = \sqrt{2\sigma/\rho_l d_b + g d_b/2}\mathrm{SF};\mathrm{SF} = \left[1 - \left(d_b/D_T\right)^2\right]^{3/2} \quad (10)$$

where V_b is the terminal velocity of the bubble (m/s), σ is the coefficient of surface tension (N/m), ρ_l is liquid density (kg/m^3), d_b is bubble diameter (mm), and D_T is the diameter of the tank (mm).

The CFD numerical model was validated using Eq. (10) which is valid for the 3–17 mm diameter of bubbles. A water tank of 50 mm diameter and air bubbles of 4 mm, 6 mm, 9 mm, and 15 mm diameter were considered for the validation study. No-slip boundary conditions were set at the top and bottom ends of the tank while free slip wall conditions were set at vertical walls. Initially, bubbles were patched at a height of 10 mm from the bottom of the tank. The time evolution of the 4-mm bubble inside the tank is represented in Fig. 4a. The comparative study resulted in an error of less than 5% between terminal velocity computed from the mathematical model and the analytical correlation for 4 mm, 6 mm, 9 mm, and 15 mm cases (Fig. 4b).

Experimental observations of gas-liquid (G-L) and liquid-liquid (L-L) immiscible interactions were taken from studies conducted by Guo and Chen (2009) and Li et al. (2010). These experiments draw relevance to this research owing to their flow profiles at low capillary numbers through microchannels, and the fact that CO_2 behaves as gas and liquid at a supercritical state. The simulation results produced a close match between the advancing interface of the dispersed phase of gas in liquid (Fig. 5a) and liquid in liquid (Fig. 5b).

Meshing details and matrices

Figure 6a illustrates a meshed geometry along with mesh matrices for the sample porous model of 160 µm × 80 µm considered for the study (also see Fig. 3). As mentioned previously, a 2-D rectangular domain with non-uniform rock matrix distribution was considered for the study. A free triangular meshing scheme was adopted for mesh generation due to highly non-linear boundaries.

A mesh sensitivity study was conducted for different mesh refinements and is depicted in Fig. 6b. The mesh refinements of 66,050 elements were considered for the study owing to their accuracy and low computational power.

Fluid properties and boundary conditions

Sc-CO_2 EOR is more effective in oil gravities higher than 25° American Petroleum Institute (API) (El-hoshoudy and Desouky 2018). In this work, two types of crude

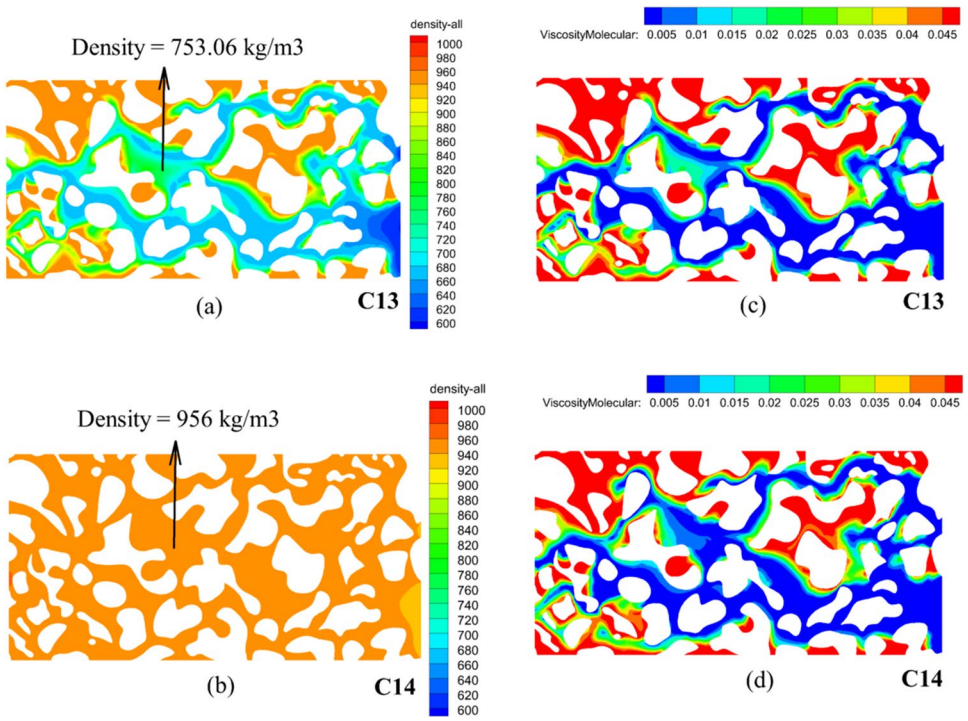

Fig. 13 **a**, **b** Density (kg/m^3) distribution of sc-CO_2 and heavy oil phase mixture at 0.05 s for **a** C13 and **b** C14. **c**, **d** Molecular viscosity (mPa/s) contour of sc-CO_2 and heavy oil phase mixture at 0.05 s for **c** C13 and **d** C14

oils (light and heavy) have been considered for sc-CO_2 EOR studies. The oil properties were adopted from Anton Paar database (Viscosity of crude oil – viscosity table and viscosity chart. Anton Paar Wiki n.d.), where the rheological parameters and density were defined for light oil (37.9° API, density 835.3 kg/m^3) and heavy oil (12.3° API, density 984 kg/m^3). A detailed value of parameters considered for this investigation is presented in Table 1. Eighteen cases of CFD simulations have been solved with varying oil viscosity, oil density, reservoir pressure, and temperature, and sc-CO_2 injection velocity (see Table 1). In this study, a multiphase VOF model was enabled for interface tracking. A very low surface tension (0.0015 N/m) was considered as sc-CO_2 acts as an effective solvent in a supercritical state although remains immiscible with a heavier fraction. This approximate value has been taken from the experimental results by Yang et al. (2015), where they used the pendant drop method and the axisymmetric drop shape analysis (ADSA) to quantify the interfacial tension between CO_2 and reservoir crude oils. Measurements were conducted at high pressures and temperatures up to 45 MPa and 412.15 K, respectively. The results reveal that, at first, the interfacial tension between CO_2 and crude oils drops rapidly as pressure is increased, and then, due to heavy components in the crude oils, the interfacial tension reduces more slowly as pressure is increased. For CO_2 + crude oil systems, there is no ultra-low or zero interfacial tension. The interfacial tensions between CO_2 and hexadecane at 318.15 K were also measured for comparison. The results reveal that the vanishing interfacial tension and miscible phenomena are found for the CO_2 + hexadecane system. Similar ultra-low IFT values can also be seen in the works of Gajbhiye (2020). Velocity inlet boundary conditions were set at the inlets, whereas outlets were set to operate reservoir pressure. The walls were modeled with no-slip boundary conditions. Thermal boundary conditions were modeled by the energy equation. Walls were set at the operating temperature (reservoir temperature, see Table 1), while the inlet was always kept at 10 K higher than the insulated wall temperature. Outlet temperature was set constant to 305 K for all the cases. Properties of sc-CO_2 were modeled using the inbuilt National Institute of Standards and Technology (NIST) dataset. A thermal lookup table was created to model the thermal properties of sc-CO_2 using the same database. Semi-Implicit Method for Pressure-Linked Equations (SIMPLE) algorithm was used for pressure-velocity coupling. An implicit formulation of the multiphase VOF model was implemented in the study. The transient approach was used to model the

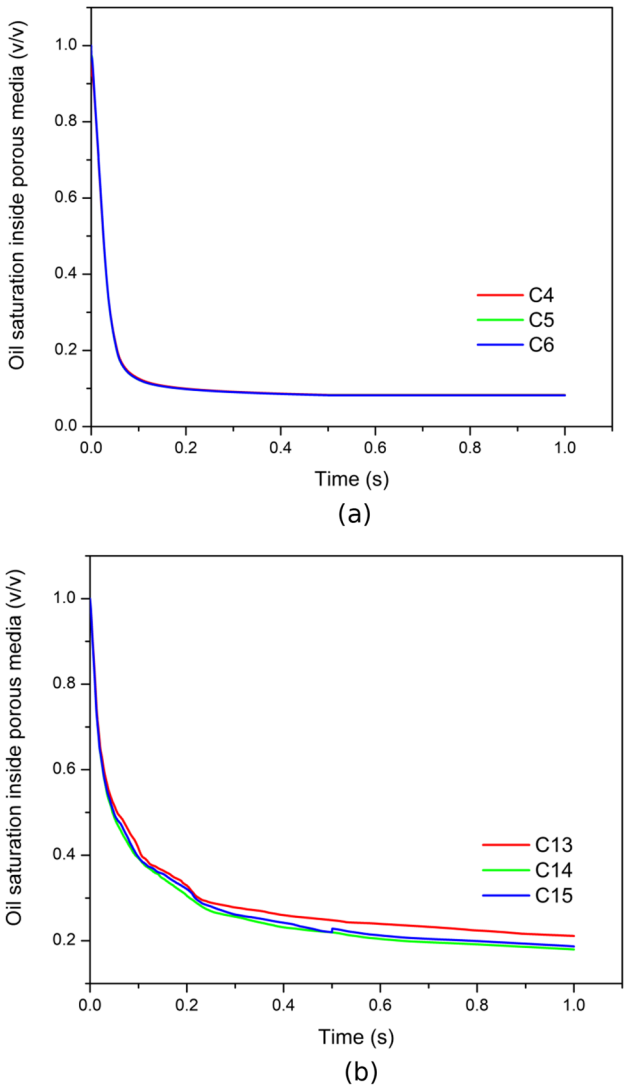

Fig. 14 Oil saturation decline curve for an sc-CO_2 inlet velocity of 0.005 m/s and different pressure and temperature conditions for **a** light oil (C4–C6) and **b** heavy oil (C13–C15)

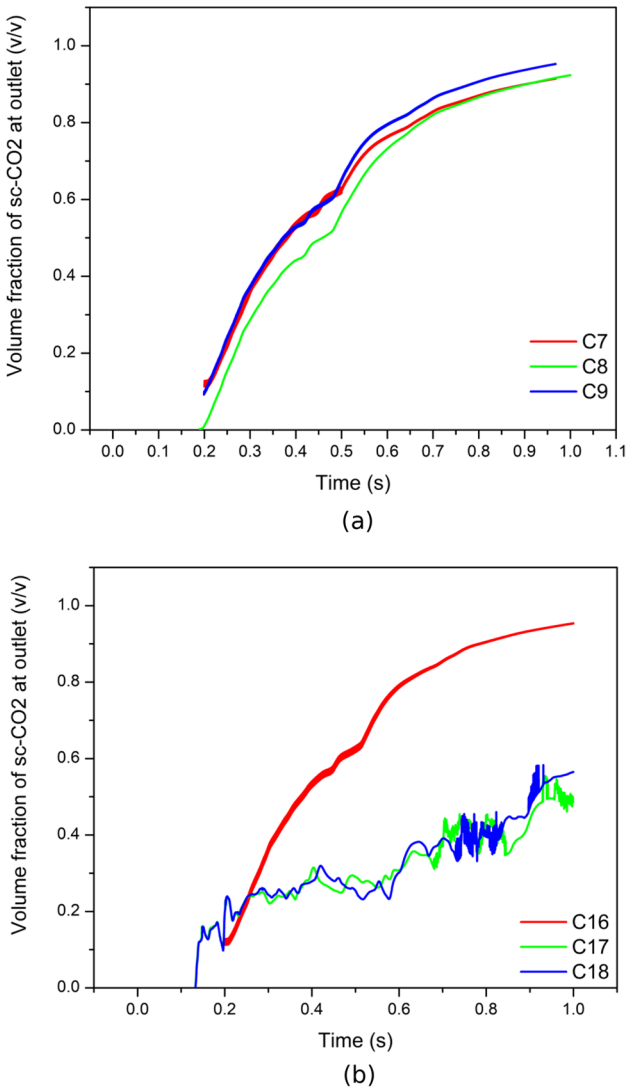

Fig. 15 Volume fraction of sc-CO_2 at the outlet for an inlet velocity of 0.0005 m/s and different pressure and temperature conditions for **a** light oil (C7–C9) and **b** heavy oil (C16–C18)

time-dependent properties. The fluid domain was initially 100% saturated with oil, and the solution was initialized from the inlet. Convergence criteria and time step size were set at 10^{-4} s and 10^{-4} s, respectively, for accurate results.

Results and discussion

The study is divided into four sets: (a) the effect of sc-CO_2 injection velocity on displacement mechanism at low pressure and temperature conditions (C1 to C3 and C10 to C12, Table 1), (b) the effect of reservoir temperature and pressure at constant high sc-CO_2 injection velocity (0.005 m/s) (C4 to C6 and C13 to C15, Table 1), (c) the effect of reservoir temperature and pressure at constant low sc-CO_2 injection velocity (0.0005 m/s) (C7 to C9 and C16 to C18, Table 1), and (d) the quantitative analysis of areal sweep before sc-CO_2 breakthrough at the outlet. The study parameters include a change in oil saturation (oil recovery), sc-CO_2 breakthrough, the interaction of sc-CO_2 and oil, physical property contour plots like viscosity and density of the sc-CO_2 and oil mixture phase, and final sc-CO_2 sequestration within the pore network.

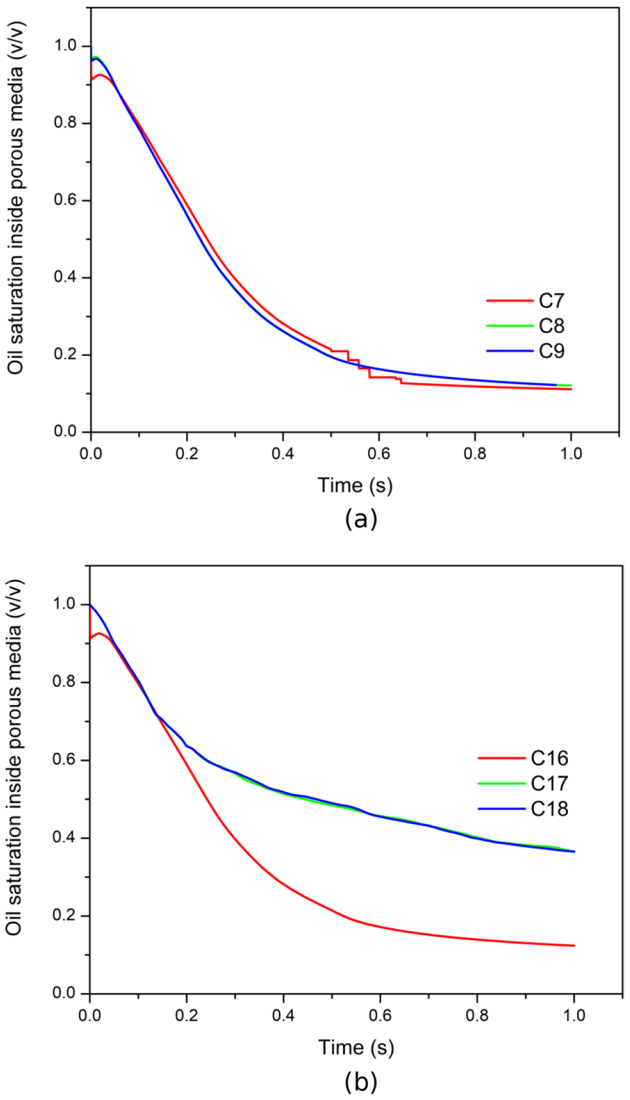

Fig. 16 Oil saturation decline curve for an inlet velocity of 0.0005 m/s and different pressure and temperature conditions for **a** light oil (C7–C9) and **b** heavy oil (C16–C18)

Effect of injection velocity on the displacement mechanism

Figure 7 represents sc-CO_2 breakthrough for the two oils undertaken in this study, i.e., light oil and heavy oil at different injection velocities. The observations were made under pressure and temperature condition of 20 MPa and 323 K (C1 to C3 and C10 to C12), respectively. The injection velocity for case nos. C1 and C10 was 0.005 m/s, that for C2 and C11 was 0.001 m/s, and that for C3 and C12 was 0.0005 m/s (Fig. 7a, b). It was observed that for higher injection velocities, sc-CO_2 residence time inside the flow domain was comparatively less. Owing to this, it led to a faster breakthrough. Additionally, at higher velocities (C1), the time difference between the outlet breakthrough and maximum breakthrough of sc-CO_2 was negligible, whereas, as the inlet velocity decreases, the rise in the volume fraction of sc-CO_2 at the outlet is rather smooth (C2 and C3). This observation indicates that areal sweep at lower injection velocities increases with time. In the former case, due to higher momentum, the path of flow would have a decreased areal influence. Furthermore, the trend of sc-CO_2 volume fraction at the outlet for heavy oil showed a non-uniform oscillatory behavior (unstable zone) at low and high velocities (Fig. 7b).

A similar observation was made when studying the contours of oil volume fraction as represented in Fig. 8a, b, and c and Fig. 9a, b, and c. It can be noticed that at an injection velocity of 0.005 m/s for light oil (C1) and heavy oil (C10), sc-CO_2 breakthroughs have already commenced at 0.05 s (Figs. 8a and 9a). At 0.05 s, an aerial sweep of light oil (C1) is higher than that of heavy oil (C10). Due to higher viscosity in the case of heavy oil (C12), an elongated viscous front can be observed as compared to light oil (C3) (Figs. 8c and 9c).

Figure 10 depicts the decline in oil saturation (v/v) corresponding to sc-CO_2 flooding at different velocities which represent oil recovery. A decline in oil saturation implies an increase in corresponding oil recovery. Both light oil (C1–C3) and heavy oil (C10–C12) showed similar behaviors towards time transient simulations with declining oil saturations. However, the total oil recovery (implied by a decrease in oil saturation) in the case of heavy oil was relatively less than that of light oil (Fig. 10a, b). The difference in ultimate recovery was significantly higher (approximately 30%) for low-velocity flooding cases (C3 and C12). The simulations with higher injection velocities (C1 and C10) showed steeper slopes for oil saturation decline due to lower residence time inside the flow domain. Additionally, the effect of change in velocity had a significant impact on the case of heavy oil as compared to light oil. This shows that oil with higher densities and viscosities (typically heavy oils) could be more sensitive towards change in injection velocities. Figure 11 shows a comparison between final sc-CO_2 sequestration for light crude oil (C1 and C3) and heavy crude oil (C10 and C12) at high (0.005 m/s) and low (0.0005 m/s) velocities. It is noteworthy to observe that the displacement of oil or sequestration of sc-CO_2 was higher for light oil at high velocities. However, the trend reverses for heavy oil due to its high density and

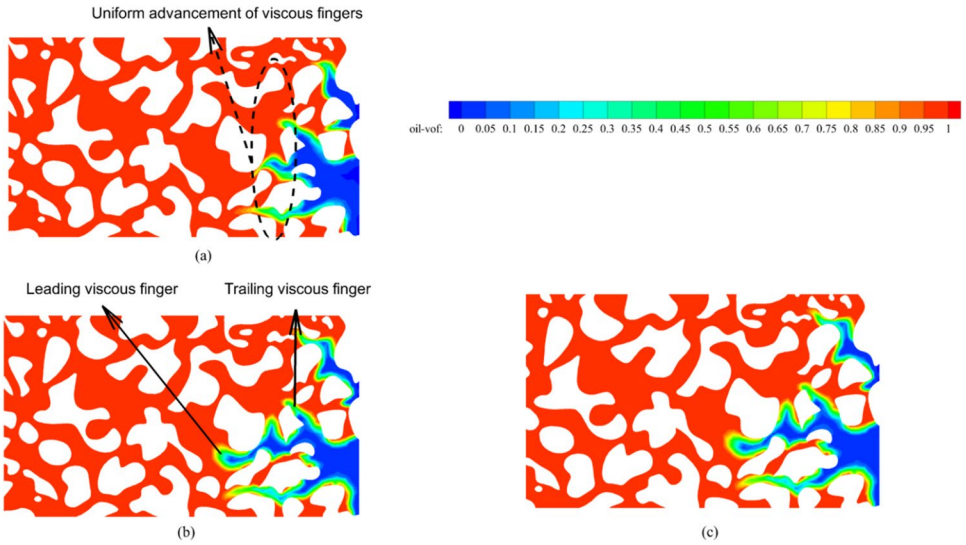

Fig. 17 Oil phase distribution at 0.05 s for heavy oil (**a** C16, **b** C17, and **c** C18) at different pressure and temperature conditions for low injection velocity (0.0005 m/s). For all the injected sc-CO_2, viscous fronts can be observed emerging from the inlet zone

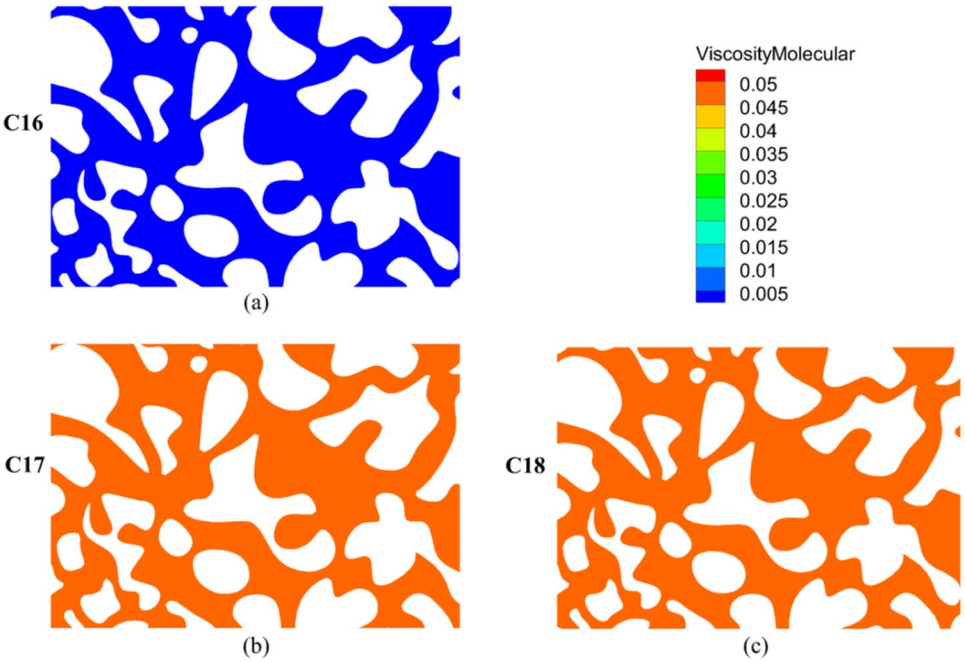

Fig. 18 Molecular viscosity contours for heavy oils (**a** C16, **b** C17, and **c** C18) at different pressure and temperature conditions for low injection velocity (0.0005 m/s). C16 displays the least in situ viscosity due to high temperature and low pressure. C18 has higher viscosity due to an increase in pressure from 20 to 40 MPa

viscosity, where sequestration of sc-CO_2 was lower at low velocities.

Effect of temperature and pressure at high injection velocity

The plots of volume fraction of sc-CO_2 at the outlet for different pressure and temperature conditions with high sc-CO_2 inlet velocity (0.005 m/s) are depicted in Fig. 12. The characteristic behavior showed a negligible effect of pressure and temperature at high injection velocities (Fig. 12a, b). The cases, viz. C4, C5, and C6, showed overlapping similar trends due to lighter viscosity of the light oil with little or no sensitivity towards varying pressure and temperature conditions at high injection velocities (Fig. 12a). However, this was not the case for heavy oil, i.e., for C14 (Fig. 12b), under high-pressure and relatively low-temperature conditions. This can be inferred from the density and viscosity contours of the sc-CO_2-oil mixture as shown in Fig. 13. At high-pressure conditions, due to the compressible nature of sc-CO_2, the density, as well as viscosity, significantly increases which leads to better compatibility with the oil (Fig. 13). It can be observed that the

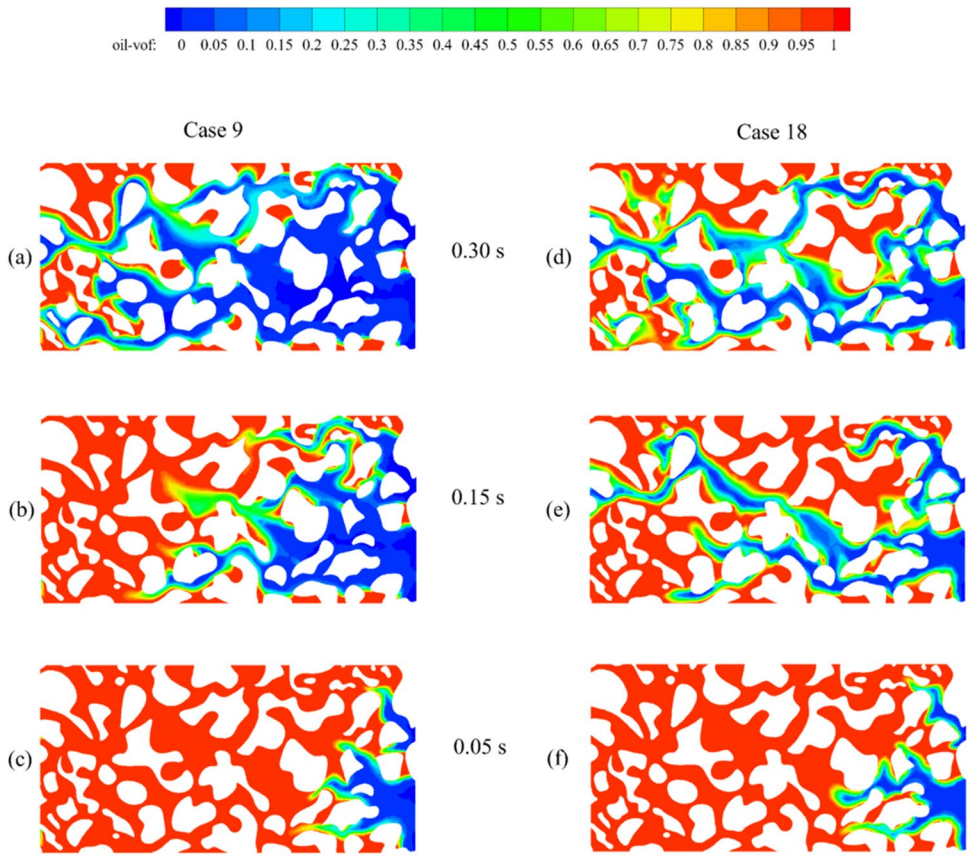

Fig. 19 Time evolution of sc-CO_2 flooding for C9 (light oil) and C18 (heavy oil). **a–f** These cases represent the same pressure, temperature, and sc-CO_2 injection velocity conditions but different oil properties

distribution in density inside the flow domain was rather uniform in the case of C14. On the contrary, C13 and C15 have relatively high-temperature regimes (see Table 1 for temperature conditions) which contribute to the decrease in density and viscosity of sc-CO_2 that yields poor mobility contrast.

As aforementioned, due to the lighter viscosity of in situ oil for light crude oil, cases C4, C5, and C6 showed a coincidental trend for oil saturation decline with the progress in sc-CO_2 flooding (Fig. 14a). However, a slightly diverse course was observed in the case of heavy oil (Fig. 14b). It can be rationalized that the effect of pressure and temperature has a greater impact on dense oil as compared to light oil. Moreover, the temperature has a detrimental effect on recovery at high injection velocities of sc-CO_2 as well. Recovery of oil in the case of C15 confirms that pressure, although marginal, offsets the adverse effect of temperature in low oil recovery.

Effect of pressure and temperature at low injection velocity

Figure 15 represents the volume fraction of sc-CO_2 at the outlet for different pressure and temperature conditions at low injection velocity (0.0005 m/s). sc-CO_2 breakthrough for light oils as represented by C7, C8, and C9 followed a similar trend (Fig. 15a). However, as compared to flow measurements at high velocities (Fig. 12a), the similarity of sc-CO_2 breakthrough was less as compared to high injection velocities. Heavy oil (C16), under

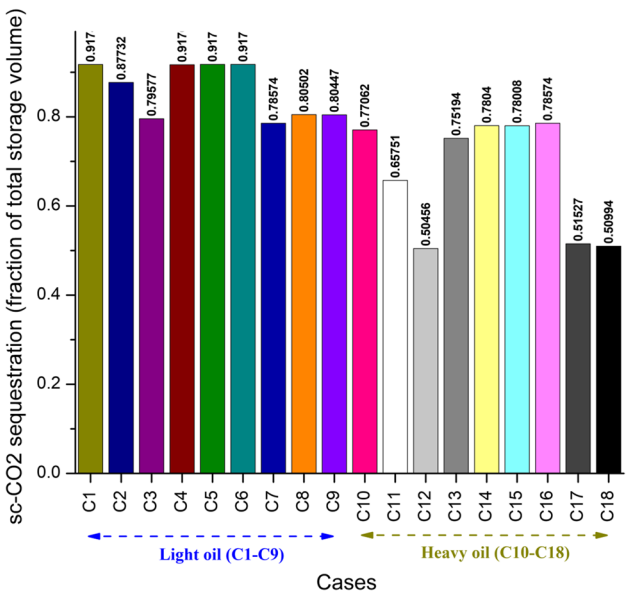

Fig. 20 Final sc-CO_2 sequestration amount for all the simulated cases

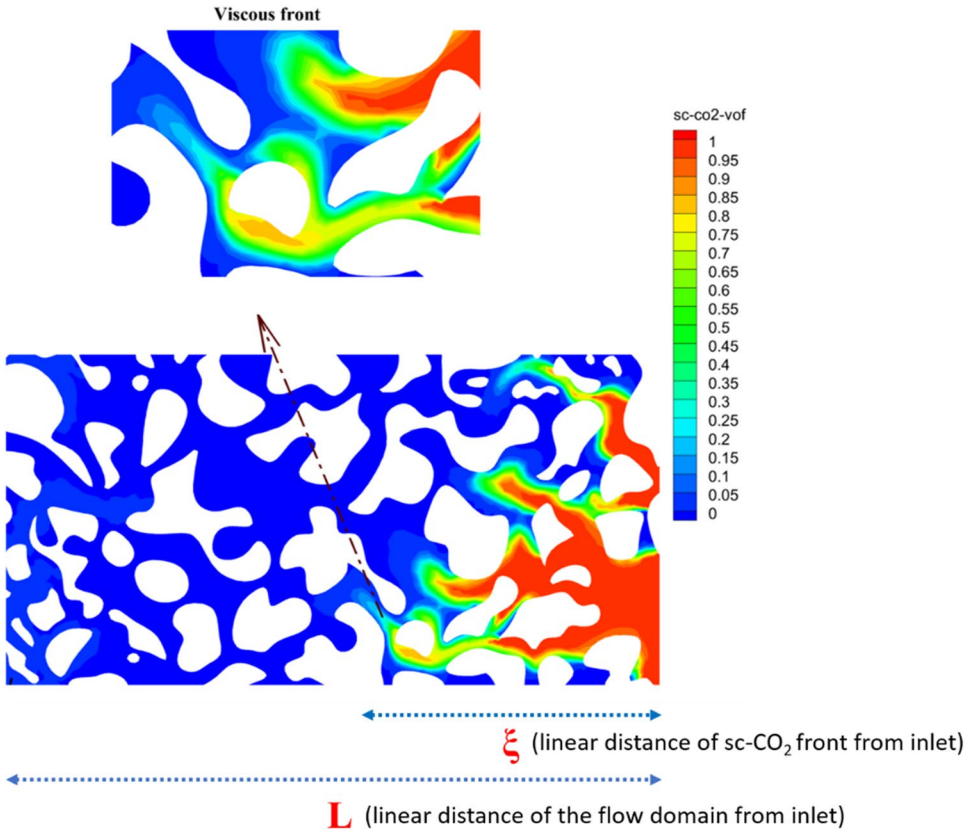

Fig. 21 An illustration of viscous front and the concept of linear normalized distance of the viscous front

high-temperature and low-pressure conditions with low injection velocity, showed a stable 90% breakthrough (having fewer fluctuations of sc-CO_2 volume fraction at the outlet) as compared to other conditions of C17 and C18 (Fig. 15b).

The decreasing oil saturation inside the flow domain was influenced by reservoir pressure and temperature as evident from Fig. 16. Figure 17 shows the oil phase distribution at 0.05 s for the same injection velocity. As compared to Fig. 14a, which represents flow conditions at high velocity, Fig. 16a shows a slight deviation especially at high-temperature conditions (C7). Additionally, in the case of heavy oil (C16, C17, and C18), the case having lower operating pressure and high temperature (C16) shows an anomalous trend as opposed to C17 and C18 (Fig. 16b). Here, the flow of CO_2 being in the supercritical phase shows negligible change towards varying temperatures at high-pressure conditions (40 MPa). This can be observed in case nos. C8, C9, C17, and C18, where high-pressure and varying temperature conditions were simulated (Fig. 16a, b). This can be noted in Fig. 17 where heavy oil in C17 and C18 (Fig. 17b, c) showed similar oil phase distribution with extended viscous fronts (high viscous fingering). However, heavy oil in case no. C16 (Fig. 17a) followed a different course (low viscous fingering) where all the vicious front covers almost the same distance with time. This significantly increases the microscopic displacement efficiency of oil for an EOR process.

Figure 18 shows the in situ molecular viscosity of oils for heavy oil (C16, C17, and C18). The reason for the similar trend for breakthrough and oil saturation decline (Fig. 15b and Fig. 16b, respectively) can be inferred from Fig. 18, where C17 and C18 showed a similar distribution in molecular viscosity. Case C16, on the other hand, showed the least viscosity owing to which the higher mobility of oil was achieved.

A comparison was made between the flooding mechanism for light and heavy crude oil under high-pressure and high-temperature conditions for low injection velocity (0.0005 m/s). This is illustrated in Fig. 19 where the time evolution of sc-CO_2 flooding for C9 and C18 is drawn. It can be seen that the sc-CO_2 front travels faster in the case of C18 which leads to a premature breakthrough at the outlet. On the other hand, C9 has a wider distribution front where sc-CO_2 shows better penetration into the individual pores owing to which the case C9 showed better residual oil recovery as compared to C18. Figure 20 represents the ultimate sc-CO_2 sequestration in the given porous media for all the considered cases. Higher CO_2 sequestrations have been observed in the case of light oils as compared to heavy oil. Additionally, at relatively

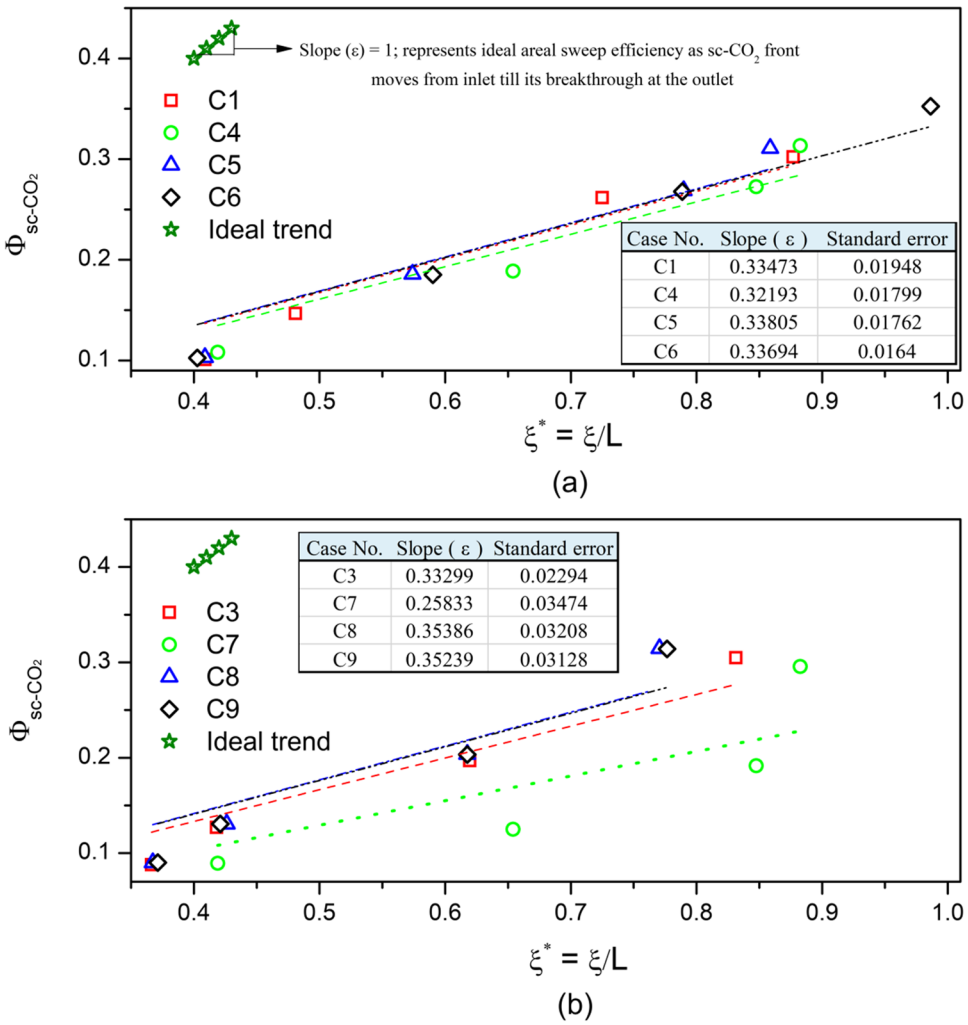

Fig. 22 Relationship between sc-CO_2 saturation and linear normalized distance of the viscous front from the inlet for light oil at **a** high (0.005 m/s) and **b** low (0.0005 m/s) velocities

low injection pressure, the sequestrated volume fraction of sc-CO_2 was higher which is confirmed by studies conducted by Abdoulghafour et al. (2020).

Quantitative analysis of areal sweep before sc-CO_2 breakthrough at the outlet

A quantitative analysis has been conducted to analyze the displacement process of oil by sc-CO_2. Displacement patterns were numerically expressed to evaluate the areal sweep of the invasion process. A new dimensionless parameter, stabilizing factor (ε) that signifies an increase in the rate of sc-CO_2 volume fraction (saturation) inside the flow domain concerning the distance of the leading sc-CO_2 front from the inlet, is introduced.

$$\varepsilon = \frac{\partial \Phi_{sc-CO_2}}{\partial \xi^*} \tag{11}$$

where Φ_{sc-CO_2} is the surface integral of the volume fraction of sc-CO_2 inside the flow domain at an instantaneous time (Eq. (8)). ξ^* is the linear normalized distance of the viscous front from the inlet expressed as

$$\xi^* = \frac{\xi}{L} \tag{12}$$

where ξ is the distance of the viscous front from the inlet and L is the linear length of the flow geometry (160 µm). The condition for a complete displacement is $\varepsilon = 1$, where the existence of the viscous front ceases (also described as compact displacement) with a flat stable front. As ε decreases (less than 1), more unstable displacement fronts are attained that signifies inferior areal sweep and unstable fluid-fluid interface (less compacted). Figure 21 presents an example of the abovementioned notion.

Figures 22 and 23 show the relationship between sc-CO_2 saturation and linear normalized distance of the viscous front from the inlet for the light oil and heavy oil reservoir. A general observation from Figs. 22 and 23 is the notable linear rise of Φ_{sc-CO_2} with an increase in ξ^*. The slope of the Φ_{sc-CO_2} and ξ^* as obtained from a linear fit yield ε, that is positive. For light oil at high velocities

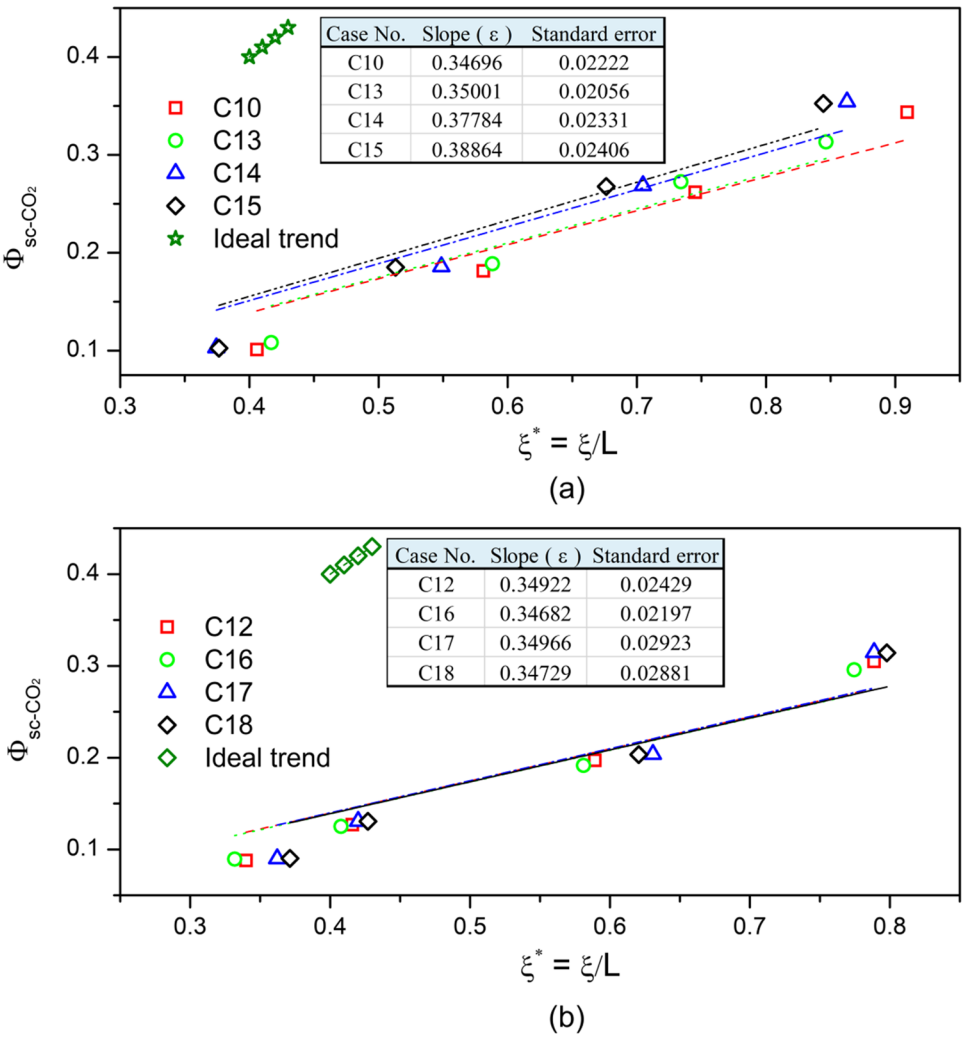

Fig. 23 Relationship between sc-CO_2 saturation and linear normalized distance of the viscous front from the inlet for heavy oil at **a** high (0.005 m/s) and **b** low (0.0005 m/s) velocities

(0.005 m/s), the stabilizing factor (ε) was observed to be almost the same (Fig. 22a). However, at low velocities (0.0005 m/s), a significant variation in ε was noticed. C7 that represents high reservoir temperature shows a poor areal sweep with a stabilizing factor (ε) of 0.25833 (Fig. 22b). Due to the greater density of sc-CO_2, the highest sweep could be noticed at high pressure (40 MPa) cases (viz., C5 and C6) that yields better mobility contrast as discussed previously.

Contrastingly, heavy oil shows a substantial variation in ε at high velocities (0.005 m/s) with high-pressure (40 MPa) cases (viz., C14 and C15) showing better stability of the moving sc-CO_2 front in terms of areal invasion (Fig. 23a). From Fig. 23b, one can observe the identical trend of sc-CO_2 invasion at low velocities (0.0005 m/s) for heavy oil. This confirms that beyond a certain magnitude of injection velocity, the invasion pattern becomes insensitive. At low velocities, the effect of pressure and temperature for heavy oil hardly carries any significance in terms of frontal advancement of the viscous front.

Conclusion

The present study evaluates different cases of sc-CO_2 as an EOR displacing fluid inside porous media with random rock matrix distribution. Reservoir temperature, reservoir pressure, oil properties, and sc-CO_2 injection velocity were the control parameters. In this study, rather than incorporating static properties of sc-CO_2, the changes in its properties due to varied reservoir pressure and temperature conditions have been captured through Helmholtz free energy equation (EOS). The effect of these control parameters was studied through oil saturation decline curve, flow front evolution, sc-CO_2 breakthrough, and final sc-CO_2 sequestration. It was concluded that sc-CO_2 miscible flooding can be an efficient

method for tertiary EOR and was more effective in the case of lighter oils. On the contrary, the recovery of heavy oil was limited but can be optimized by varying the injection sc-CO_2 velocity. At high-pressure conditions, the effect of temperature was not very significant. For heavy oil, an optimal operation point (injection velocity) can be obtained by maintaining a favorable viscosity contrast and promote better oil displacement and sc-CO_2 sequestration.

The main conclusions from the study can be summarized in the following points:

- The breakthrough volume fraction of sc-CO_2 at the outlet showed smooth profiles at low pressure (20 MPa) and low temperature (323 K) for light oil at high velocities. However, it showed fluctuations in the case of heavy oil.
- Optimum shear force must be generated for uniform flow after sc-CO_2 breakthrough which was observed for both light oil and heavy oil at 0.001 m/s injection velocities.
- The effect of change in velocity had a significant impact on the case of heavy oil as compared to light oil. This shows that oil with higher densities and viscosities could be more sensitive towards change in injection velocities.
- At high injection velocities, sc-CO_2 breakthrough, as well as oil recovery for light oil, was not sensitive to change in pressure and temperature. On the other hand, heavy oil showed marginal differences.
- At low injection velocities (0.0005 m/s), the flow of CO_2 being in the supercritical phase shows negligible change towards varying temperatures at high-pressure conditions. Additionally, at lower velocity, for heavy oil, the extent of viscous fingering is less at high temperatures, which eventually increases microscopic displacement efficiency.
- The effectiveness of sc-CO_2 in displacing light oil was more prominent as a result of a wider displacing front.
- Cases of higher velocity seem to have a more unified (insensitive) frontal behavior than low velocity cases for light oils. However, for heavy oil, cases of lower injection velocity have a more unified sc-CO_2 front pattern. It can be assumed that a velocity threshold is not the only decisive factor and oil type is also a parameter at play.
- The effectiveness of the invasion pattern of sc-CO_2 was expressed in terms of a new dimensionless number (ε) known as stabilizing factor. It was observed that ε for light oil was highly affected at lower velocities (0.0005 m/s). However, for heavy oil, the relationship was reversed that showed sensitivity at lower velocities (0.005 m/s) as compared to higher ones (0.005 m/s).
- The effect of mass transfer between pre-injected brine, sc-CO_2, and oil on the flow characteristics and oil recovery shall be investigated in future studies.

Author contribution Conceptualization: Dr. Jitendra S. Sangwai and Satyajit Chowdhury; methodology: Satyajit Chowdhury and Mayank Rakesh; formal analysis and investigation: Satyajit Chowdhury, Mayank Rakesh, and Dr. Srawanti Medhi; writing (original draft preparation): Satyajit Chowdhury and Mayank Rakesh; writing with review and editing: Dr. Jitendra S. Sangwai, Dr. Japan Trivedi, and Dr. Srawanti Medhi; supervision: Dr. Jitendra S. Sangwai

Availability of data and materials All data generated or analyzed during this study are included in this published article.

Declarations

Ethics approval and consent to participate Not applicable

Consent for publication Not applicable

Competing interests The authors declare no competing interests.

References

Abdoulghafour H, Sarmadivaleh M, Hauge LP, Fernø M, Iglauer S (2020) Capillary pressure characteristics of CO_2-brine-sandstone systems. Int J Greenh Gas Control 94:102876. https://doi.org/10.1016/j.ijggc.2019.102876

Ahmadi MA, Pouladi B, Barghi T (2016) Numerical modeling of CO_2 injection scenarios in petroleum reservoirs: application to CO_2 sequestration and EOR. J Nat Gas Sci Eng 30:38–49. https://doi.org/10.1016/j.jngse.2016.01.038

Alvarado V, Eduardo M (2010) ENHANCED OIL RECOVERY Field Planning and Development. Gulf Professional Publishing

Al-Zaidi E, Fan X, Edlmann K (2018) Supercritical CO2 behaviour during water displacement in a sandstone core sample. Int J Greenh Gas Control 79:200–211. https://doi.org/10.1016/j.ijggc.2018.11.005

ANSYS (2009) Heat transfer theory. ANSYS Inc. https://www.afs.enea.it/project/neptunius/docs/fluent/html/th/node107.htm. Accessed 15 Apr 2022

Azzolina NA, Peck WD, Hamling JA, Gorecki CD, Ayash SC, Doll TE, Nakles DV, Melzer LS (2016) How green is my oil? A detailed look at greenhouse gas accounting for CO2-enhanced oil recovery (CO2-EOR) sites. Int J Greenh Gas Control 51:369–379. https://doi.org/10.1016/j.ijggc.2016.06.008

Bachu S (2000) Sequestration of CO_2 in geological media: Criteria and approach for site selection in response to climate change. Energy Convers Manag 41:953–970. https://doi.org/10.1016/S0196-8904(99)00149-1

Behera US, Sangwai JS (2020) Synergistic effect of brine system containing mixed monovalent (NaCl, KCl) and divalent ($MgCl_2$, $MgSO_4$) salts on the interfacial tension of pure hydrocarbon-brine system relevant for low salinity water flooding. Energy Fuel 34:4201–4212. https://doi.org/10.1021/acs.energyfuels.9b04525

Brackbill JU, Kothe DB, Zemach C (1992) A continuum method for modeling surface tension. J Comput Phys 100:335–354. https://doi.org/10.1016/0021-9991(92)90240-Y

Carbon dioxide - gas encyclopedia air liquide | air liquide (n.d.) [WWW document]

Choi HS, Park HC, Huh C, Kang SG (2011) Numerical simulation of fluid flow and heat transfer of supercritical CO_2 in micro-porous media. Energy Procedia 4:3786–3793. https://doi.org/10.1016/j.egypro.2011.02.313

Clemens T, Tsikouris K, Buchgraber M, Castanier L, Kovscek A (2013) Pore-scale evaluation of polymers displacing viscous oil-computational- fluid-dynamics simulation of micromodel experiments. SPE Reserv Eval Eng 16:144–154. https://doi.org/10.2118/154169-PA

Connolly PRJ, Vogt SJ, Iglauer S, May EF, Johns ML (2017) Capillary trapping quantification in sandstones using NMR relaxometry. Water Resour Res 53:7917–7932. https://doi.org/10.1002/2017WR020829

El-hoshoudy AN, Desouky S (2018) CO2 miscible flooding for enhanced oil recovery. In: Carbon capture, utilization and sequestration. IntechOpen, pp 79–93. https://doi.org/10.5772/intechopen.79082

Enick RM, Olsen D, Ammer J, Schuller W (2012) Mobility and conformance control for CO_2 EOR via thickeners, foams, and gels - a literature review of 40 years of research and pilot tests. SPE - DOE Improv. Oil Recover Symp Proc 2:910–921. https://doi.org/10.2118/154122-ms

Fanchi JR (2010) Reservoir simulation. In: In: Integrated reservoir asset management. Elsevier, Amsterdam, pp 223–241. https://doi.org/10.1016/B978-0-12-382088-4.00013-X

Gajbhiye R (2020) Effect of CO_2/N_2 mixture composition on interfacial tension of crude oil. ACS Omega 5:27944–27952. https://doi.org/10.1021/acsomega.0c03326

Gaspar Ravagnani ATFS, Ligero EL, Suslick SB (2009) CO_2 sequestration through enhanced oil recovery in a mature oil field. J Pet Sci Eng 65:129–138. https://doi.org/10.1016/j.petrol.2008.12.015

Gharibshahi R, Jafari A, Haghtalab A, Karambeigi MS (2015) Application of CFD to evaluate the pore morphology effect on nanofluid flooding for enhanced oil recovery. RSC Adv 5:28938–28949. https://doi.org/10.1039/c4ra15452e

Gharibshahi R, Jafari A, Ahmadi H (2019) CFD investigation of enhanced extra-heavy oil recovery using metallic nanoparticles/steam injection in a micromodel with random pore distribution. J Pet Sci Eng 174:374–383. https://doi.org/10.1016/j.petrol.2018.10.051

Green DW, Willhite GP (1998) Enhanced oil recovery, SPE textbo. Richardson, TX: Henry L. Doherty Memorial Fund of AIME, Society of Petroleum Engineers

Guo F, Chen B (2009) Numerical study on taylor bubble formation in a micro-channel t-junction using vof method. Microgr Sci Technol 21:51–58. https://doi.org/10.1007/s12217-009-9146-4

Guo Y, Zhang L, Zhu G, Yao J, Sun H, Song W, Yang Y, Zhao J (2019) A pore-scale investigation of residual oil distributions and enhanced oil recovery methods. Energies 12:3732. https://doi.org/10.3390/en12193732

Hargreaves DM, Morvan HP, Wright NG (2007) Validation of the volume of fluid method for free surface calculation: the broad-crested weir. Eng Appl Comput Fluid Mech 1:136–146. https://doi.org/10.1080/19942060.2007.11015188

Hashemi Fath A, Pouranfard AR (2014) Evaluation of miscible and immiscible CO_2 injection in one of the Iranian oil fields. Egypt J Pet 23:255–270. https://doi.org/10.1016/j.ejpe.2014.08.002

He D, Jiang P, Lun Z, Liu X, Xu R (2019) Pore scale CFD simulation of supercritical carbon dioxide drainage process in porous media saturated with water. Energy Sources. Part A Recover Util Environ Eff 41:1791–1799. https://doi.org/10.1080/15567036.2018.1549155

Hill LB, Li X, Wei N (2020) CO_2-EOR in China: a comparative review. Int J Greenh Gas Control 103:103173. https://doi.org/10.1016/j.ijggc.2020.103173

Hirt C, Nichols B (1981) Volume of fluid (VOF) method for the dynamics of free boundaries. J Comput Phys 39:201–225. https://doi.org/10.1016/0021-9991(81)90145-5

Huppert HE, Neufeld JA (2014) The fluid mechanics of carbon dioxide sequestration. Annu Rev Fluid Mech 46:255–272. https://doi.org/10.1146/annurev-fluid-011212-140627

Iglauer S, Paluszny A, Pentland CH, Blunt MJ (2011) Residual CO_2 imaged with X-ray micro-tomography. Geophys Res Lett 38:n/a. https://doi.org/10.1029/2011GL049680

Iglauer S, Rahman T, Sarmadivaleh M, Al-Hinai A, Fernø MA, Lebedev M (2016) Influence of wettability on residual gas trapping and enhanced oil recovery in three-phase flow: a pore-scale analysis by use of microcomputed tomography. SPE J 21:1916–1929. https://doi.org/10.2118/179727-PA

Iglauer S, Paluszny A, Rahman T, Zhang Y, Wülling W, Lebedev M (2019) Residual trapping of CO_2 in an oil-filled, oil-wet sandstone core: results of three-phase pore-scale imaging. Geophys Res Lett 46:11146–11154. https://doi.org/10.1029/2019GL083401

IPCC (2006) Carbon dioxide capture and storage: special report of the Intergovernmental Panel on Climate Change. Cambridge University Press, Cambridge

Jeong W, Seong J (2014) Comparison of effects on technical variances of computational fluid dynamics (CFD) software based on finite element and finite volume methods. Int J Mech Sci 78:19–26. https://doi.org/10.1016/j.ijmecsci.2013.10.017

Jha NK, Lebedev M, Iglauer S, Sangwai JS, Sarmadivaleh M (2020) In situ wettability investigation of aging of sandstone surface in alkane via X-ray microtomography. Energies 13:11–16. https://doi.org/10.3390/en13215594

Kakati A, Kumar G, Sangwai JS (2020) Low salinity polymer flooding: effect on polymer rheology, injectivity, retention, and oil recovery efficiency. Energy Fuel 34:5715–5732. https://doi.org/10.1021/acs.energyfuels.0c00393

Khalde CM, Samad A, Sangwai JS (2019) Computational and experimental study of sand entrapment in a hydrocyclone during desanding operations in oil fields: consequences for leakage and separation efficiency. SPE Prod Oper 34:520–535. https://doi.org/10.2118/195693-PA

Krishna R, Urseanu MI, van Baten JM, Ellenberger J (1999) Wall effects on the rise of single gas bubbles in liquids. Int Commun Heat Mass Transf 26:781–790. https://doi.org/10.1016/S0735-1933(99)00066-4

Kumar G, Kakati A, Mani E, Sangwai JS (2020) Stability of nanoparticle stabilized oil-in-water Pickering emulsion under high pressure and high temperature conditions: comparison with surfactant stabilized oil-in-water emulsion. J Dispers Sci Technol 1–14. https://doi.org/10.1080/01932691.2020.1730888

Kuuskraa VA, Van Leewen T, Wallace M (2011) Improving domestic energy security and lowering CO2 emissions with "Next Generation" CO2-Enhanced Oil Recovery (CO2-EOR). Dep Energy's OSTIIGOV. https://doi.org/10.2172/1503260

Li X-B, Li F-C, Kinoshita H, Oishi M, Oshima M (2010) Formation of uniform plugs and monodispersed droplets for viscoelastic fluid flow in microchannels. In: In: Earth and Space 2010. American Society of Civil Engineers, Reston, pp 2207–2216. https://doi.org/10.1061/41096(366)203

Li L, Yao J, Li Y, Wu M, Zhang L (2016) Pressure-transient analysis of CO_2 flooding based on a compositional method. J Nat Gas Sci Eng 33:30–36. https://doi.org/10.1016/j.jngse.2016.04.062

Li X, Li G, Wang H, Tian S, Song X, Lu P, Wang M (2017) A unified model for wellbore flow and heat transfer in pure CO_2 injection for geological sequestration, EOR and fracturing operations. Int J Greenh Gas Control 57:102–115. https://doi.org/10.1016/j.ijggc.2016.11.030

Li P, Yi L, Liu X, Hu G, Lu J, Zhou D, Hovorka S, Liang X (2019) Screening and simulation of offshore CO2-EOR and storage: a case study for the HZ21-1 oilfield in the Pearl River Mouth Basin, Northern South China Sea. Int J Greenh Gas Control 86:66–81. https://doi.org/10.1016/j.ijggc.2019.04.015

Liu J, Sun L, Li Z, Wu X (2019) Experimental study on reducing CO_2–oil minimum miscibility pressure with hydrocarbon agents. Energies 12:1975. https://doi.org/10.3390/en12101975

Lv M, Wang S (2015) Pore-scale modeling of a water/oil two-phase flow in hot water flooding for enhanced oil recovery. RSC Adv 5:85373–85382. https://doi.org/10.1039/c5ra12136a

Marchetti C (1977) On geoengineering and the CO_2 problem. Clim Chang 1:59–68. https://doi.org/10.1007/BF00162777

Markewitz P, Kuckshinrichs W, Leitner W, Linssen J, Zapp P, Bongartz R, Schreiber A, Müller TE (2012) Worldwide innovations in the development of carbon capture technologies and the utilization of CO_2. Energy Environ Sci 5:7281–7305. https://doi.org/10.1039/c2ee03403d

Martin DF, Taber JJ (1992) Carbon dioxide flooding. J Pet Technol 44:396–400. https://doi.org/10.2118/23564-PA

Medhi S, Chowdhury S, Bhatt N, Gupta DK, Rana S, Sangwai JS (2020a) Analysis of high performing graphene oxide nanosheets based non-damaging drilling fluids through rheological measurements and CFD studies. Powder Technol. https://doi.org/10.1016/j.powtec.2020.08.053

Medhi S, Chowdhury S, Kumar A, Gupta DK, Aswal Z, Sangwai JS (2020b) Zirconium oxide nanoparticle as an effective additive for non-damaging drilling fluid: a study through rheology and computational fluid dynamics investigation. J Pet Sci Eng 187:106826. https://doi.org/10.1016/j.petrol.2019.106826

Mendelson HD (1967) The prediction of bubble terminal velocities from wave theory. AICHE J 13:250–253. https://doi.org/10.1002/aic.690130213

Molina-Aiz FD, Fatnassi H, Boulard T, Roy JC, Valera DL (2010) Comparison of finite element and finite volume methods for simulation of natural ventilation in greenhouses. Comput Electron Agric 72:69–86. https://doi.org/10.1016/j.compag.2010.03.002

Moukalled F, Mangani L, Darwish M (2016) The finite volume method in computational fluid dynamics: fluid mechanics and its applications. Springer, Cham. https://doi.org/10.1007/978-3-319-16874-6_21

Nikolai P, Rabiyat B, Aslan A, Ilmutdin A (2019) Supercritical CO_2: properties and technological applications - a review. J Therm Sci. https://doi.org/10.1007/s11630-019-1118-4

Ning Y, Jin B, Liang Y, Qin G (2019) Pore-scale modeling and simulation in shale gas formations. In: In: Petrophysical characterization and fluids transport in unconventional reservoirs. Elsevier, Amsterdam, pp 217–246. https://doi.org/10.1016/B978-0-12-816698-7.00011-5

Nwidee LN, Theophilus S, Barifcani A, Sarmadivaleh M, Iglauer S (2016) EOR processes, opportunities and technological advancements. In: Chemical Enhanced Oil Recovery (cEOR) - a practical overview. IntechOpen. https://doi.org/10.5772/64828

Peach J, Eastoe J (2014) Supercritical carbon dioxide: a solvent like no other. Beilstein J Org Chem 10:1878–1895. https://doi.org/10.3762/bjoc.10.196

Pipich V, Schwahn D (2020) Polymorphic phase transition in liquid and supercritical carbon dioxide. Sci Rep 10:11861. https://doi.org/10.1038/s41598-020-68451-y

Prüss J, Simonett G (2010) On the two-phase Navier-Stokes equations with surface tension. Interfaces Free Bound 12:311–345. https://doi.org/10.4171/IFB/237

Rutqvist J (2012) The geomechanics of CO_2 storage in deep sedimentary formations. Geotech Geol Eng 30:525–551. https://doi.org/10.1007/s10706-011-9491-0

Safi R, Agarwal RK, Banerjee S (2016) Numerical simulation and optimization of CO_2 utilization for enhanced oil recovery from depleted reservoirs. Chem Eng Sci 144:30–38. https://doi.org/10.1016/j.ces.2016.01.021

Sagir M, Mushtaq M, Tahir MS, Tahir MB, Ullah S, Abbas N, Pervaiz M (2018) CO2 capture, storage, and enhanced oil recovery applications. In: In: Encyclopedia of renewable and sustainable materials. Elsevier, Netherlands, pp 52–58. https://doi.org/10.1016/B978-0-12-803581-8.10360-1

Sakthipriya N, Doble M, Sangwai JS (2016) Influence of thermophilic Bacillus subtilis YB7 on the biodegradation of long chain paraffinic hydrocarbons (C16H34 to C36H74). RSC Adv 6:82541–82552. https://doi.org/10.1039/C6RA18774A

Seetharaman GR, Jadhav RM, Sangwai JS (2020) Effect of monovalent and divalent alkali [NaOH and $Ca(OH)_2$] on the interfacial tension of pure hydrocarbon-water systems relevant for enhanced oil recovery. J Pet Sci Eng 197:107892. https://doi.org/10.1016/j.petrol.2020.107892

Sharma SS (2011) Determinants of carbon dioxide emissions: empirical evidence from 69 countries. Appl Energy 88:376–382. https://doi.org/10.1016/j.apenergy.2010.07.022

Sharma T, Iglauer S, Sangwai JS (2016) Silica nanofluids in an oilfield polymer polyacrylamide: interfacial properties, wettability alteration, and applications for chemical enhanced oil recovery. Ind Eng Chem Res 55:12387–12397. https://doi.org/10.1021/acs.iecr.6b03299

Span R, Wagner W (1996) A new equation of state for carbon dioxide covering the fluid region from the triple-point temperature to 1100 K at pressures up to 800 MPa. J Phys Chem Ref Data 25:1509–1596. https://doi.org/10.1063/1.555991, https://doi.org/10.5772/64828

Tunio SQ, Tunio AH, Ghirano NA, El Adawy ZM (2011) Comparison of different enhanced oil recovery techniques for better oil productivity. Int J Appl Sci Technol 1:143–153

van der Meer LGHB, Hofstee C, Orlic B (2009) The fluid flow consequences of CO_2 migration from 1000 to 600 metres upon passing the critical conditions of CO_2. Energy Procedia 1:3213–3220. https://doi.org/10.1016/j.egypro.2009.02.105

Viscosity of crude oil – viscosity table and viscosity chart. (n.d.) Anton Paar Wiki [WWW document]

Wang P, Zhao F, Hou J, Lu G, Zhang M, Wang Z (2018) Comparative analysis of CO_2, N_2, and gas mixture injection on asphaltene deposition pressure in reservoir conditions. Energies 11:2483. https://doi.org/10.3390/en11092483

Wang H, Li G, Zhu B, Sepehrnoori K, Shi L, Zheng Y, Shi X (2019) Key problems and solutions in supercritical CO2 fracturing technology. Front Energy 13:667–672. https://doi.org/10.1007/s11708-019-0626-y

Witkowski A, Majkut M, Rulik S (2014) Analysis of pipeline transportation systems for carbon dioxide sequestration. Arch Thermodyn 35:117–140. https://doi.org/10.2478/aoter-2014-0008

Xie X, Economides MJ (2009) The impact of carbon geological sequestration. SPE Am. E P Environ. Saf Conf 2009:50–62. https://doi.org/10.2118/120333-ms

Xu L, Li Q, Myers M, White C, Tan Y (2020) Experimental and numerical investigation of supercritical CO_2 migration in sandstone with multiple clay interlayers. Int J Greenh Gas Control 104:103194. https://doi.org/10.1016/j.ijggc.2020.103194

Yang Z, Liu X, Hua Z, Ling Y, Li M, Lin M, Dong Z (2015) Interfacial tension of CO_2 and crude oils under high pressure and temperature. Colloids Surf A Physicochem Eng Asp 482:611–616. https://doi.org/10.1016/j.colsurfa.2015.05.058

Yernazarova A, Kayirmanova G, Zhubanova ABa (2016) Microbial enhanced oil recovery. In: Chemical Enhanced Oil Recovery (cEOR) - a practical overview. Intech Open. https://doi.org/10.5772/64805

Zhang C, Qiao C, Li S, Li Z (2018) The effect of oil properties on the supercritical CO2 diffusion coefficient under tight reservoir conditions. Energies 11:1495. https://doi.org/10.3390/en11061495

Zhao J, Wen D (2017) Pore-scale simulation of wettability and interfacial tension effects on flooding process for enhanced oil recovery. RSC Adv 7:41391–41398. https://doi.org/10.1039/C7RA07325A

Zhu G, Yao J, Li A, Sun H, Zhang L (2017) Pore-scale investigation of carbon dioxide-enhanced oil recovery. Energy Fuel 31:5324–5332. https://doi.org/10.1021/acs.energyfuels.7b00058